

Accepted for ApJ. Tentatively scheduled for Dec. 20, 2000

DIFFERENTIAL O AND Si ABUNDANCES IN M33 EARLY B SUPERGIANTS

M. I. Monteverde¹, A. Herrero^{1,2},

and

D. J. Lennon³

Received date; accepted date

ABSTRACT

We present non-LTE analyses of four M33 early B-supergiant stars and five Galactic counterparts. This is the first time that B supergiants beyond the Magellanic Clouds are analyzed by means of detailed Non-LTE techniques. Among the M33 stars, new spectroscopic observations of B38 (ob21–108) are presented and the object is classified as B1Ia. The classification of another M33 star, B133, is changed with respect to a former study. Equivalent widths of O and Si lines are measured for the M33 objects. Stellar temperatures, gravities, microturbulences and Si abundances are derived for all objects using the Si ionization equilibrium and the Balmer line wings. O abundances are then also derived. Important approximations made during the calculations are described, and their influence on the results is analyzed (namely, we set the Lyman resonance lines in detailed balance during the calculation of the atmospheric structure for stars cooler than 20 000 K, and set the Si III resonance lines in detailed balance during the line formation calculations for all models). It is found that these approximations have no significant effect on the results at any microturbulence. We found a difference in the derived temperatures of the earlier Galactic stars as compared to those obtained by other authors, which we attribute to the different lines used for their derivation. A difference can also be present in the results when using the Si II/Si III and the Si III/Si IV ionization equilibria. We conclude that a strict differential analysis is needed to detect abundance differences. Thus we compare results line by line in M33 and Galactic stars of stellar parameters as similar as possible. Three of the four M33 stars turned out to be O deficient as compared to their Galactic counterparts, and only one, close to the center of M33 (M33 1054) is found to be moderately O enriched. From these differential analyses we find that our data are compatible with a radial O gradient in M33 as that derived from H II region data: we obtain -0.19 ± 0.13 or -0.20 ± 0.07 dex kpc^{-1} , depending on whether B133 is included or not. Our data are also consistent with other possibilities such

¹Instituto de Astrofísica de Canarias, E-38200 La Laguna, Tenerife, Spain

²Departamento de Astrofísica, Universidad de La Laguna, Avda. Astrofísico Francisco Sánchez, s/n, E-38071 La Laguna, Spain

³Isaac Newton Group of Telescopes, Apartado de Correos 368, E-38700 Santa Cruz de La Palma, Spain

as a steep increase of the O abundance in the inner region (at projected distances less than 9 arcmin from the center of M33), followed by a flat O abundance profile towards the outer parts of M33. Si shows the same pattern, and it is shown that Si and O correlate well, as expected for α -elements, supporting then the high value of the O abundance gradient in M33 as compared to the Milky Way and other nearby spiral galaxies. The results are compared with those of a more approximate technique, and it is concluded that this last can be used, attention being drawn to certain problems that are indicated. As an important additional point, it is shown that M33 1054 is most probably a single object, in spite of the bright absolute magnitude found in the literature.

Subject headings: galaxies: abundances — galaxies: individual(M33) — stars: abundances — stars: early-type — stars: fundamental parameters — supergiants

1. Introduction

Extragalactic stellar astrophysics, the study of individual stars in other galaxies, has been getting a strong impulse in recent years (see Massey (1998) and Kudritzki (1998) for recent reviews on the subject). The extension of spectroscopic techniques appropriate for stars in our Galaxy to those in other galaxies (in particular, beyond the Magellanic Clouds) is difficult not only because of the faintness of the stars and the related difficulty of the observations, but also because of the lack of adequate stellar classification schemes (see Lennon (1997); Monteverde et al. (1996), hereafter Paper I) and the fact that we will tend to pick up the brightests and most extreme objects, for which we lack adequate Galactic comparison standards.

In spite of all these difficulties this study is of great interest for a number of astrophysical problems. Derivation of individual stellar abundances in spiral galaxies will allow us to get radial chemical abundances of a large number of elements present in the spectra of blue supergiants, from alpha to iron-group and s-process elements, therefore giving us invaluable information about the chemical evolution of the galaxy. The wind momentum-luminosity relationship (WLR, see Puls et al. (1996) or Kudritzki et al. (1999)), a purely spectroscopic technique that can allow us to derive extragalactic distances, can be calibrated against metallicity using stars in other galaxies, especially in spirals where we can find different metallicities in the same system, avoiding uncertainties in the distance moduli. Finally, stellar evolution can be studied in different environments, in particular of different metallicities, where we can compare the number of stars in a given evolutionary status and their atmospheric properties and chemical abundances, thus helping us to disentangle the role of rotation and metallicity in internal mixing processes (see, for example, Maeder & Meynet (2000); Maeder (1999); Maeder & Zahn (1998); Maeder et al. (1999); Venn (1999); Heger (1998); Herrero et al. (1999)).

All these studies require observations of faint stars with large telescopes, as we did in Paper I, where details concerning the observations and classification problems can be found. They also require time-consuming model atmosphere calculations to get the stellar parameters and chemical abundances. In Monteverde et al. ((1997), hereafter Paper II) we derived the O abundances of B supergiants in M33 and the Milky Way by first classifying the M33 stars and selecting their Galactic counterparts among the stars ob-

served by Lennon et al. (1992) by requiring that they have the same spectral type and luminosity class. We then adopted a spectral classification—stellar parameters calibration from which T_{eff} was obtained, and derived gravity, microturbulence (again in an approximate way) and O abundance. This approximate technique allowed us to obtain the O radial abundance gradient for stars in M33. Our results were in good agreement with those for H II regions (Henry & Howard (1995)). However, this technique had several serious approximations, and it is important to confirm its applicability if we want to extend it to stars in further galaxies, particularly beyond the Local Group (with the new 8-m class telescopes, McCarthy et al. (1997) estimate that it will be possible to apply spectroscopic methods to individual stars at 20 Mpc).

In Section 2 we present the observations. Section 3 is dedicated to a description of the calculations, and Section 4 to the derived model parameters and abundances. Section 5 presents a discussion of problems and aspects of interest encountered in the individual analyses, and the discussion of the results is presented in Section 6. Finally, our conclusions are given in Section 7.

2. The observations

The stars used for the present work have been selected among the objects we have observed until now in different observing runs at La Palma using the 4.2-m William Herschel Telescope and ISIS spectrograph. The spectral resolution is about 2 Å. This resolution is not optimal, but adequate for the present analysis, based on strong isolated lines in B supergiants, which typically rotate quickly compared with cooler spectral types. Each star has been observed in two wavelength regions; the blue region (4000–4600 Å) contains most of the features needed to classify and analyze B-type supergiants. The other region is that of H α , which is a luminosity-sensitive and also a wind-diagnostic line. Details of the observations and spectral reductions, as well as plots of the stellar spectra, can be found in Paper I.

Spectral classification of M33 stars is not as easy as might be expected because of variations in metallicity and lack of adequate comparison standards. Three of the stars analyzed here were classified by Montevede et al. (1996), where these problems are discussed, and were included in our determination of the radial O gradient of M33 in Paper II. One of the stars used in Paper II has been excluded here (M33 1354) because it is too cool for the Si ionization balance to be used as temperature indicator. We have replaced it with B38, an early B supergiant that we have classified as B1Ia, following the criteria described in Paper I (more details are given in § 5). Figure 7 displays the blue spectra of our M33 stars, and Figure 7 displays the H α part of the spectra.

The Galactic standard spectra we use here have been selected from the sample by Lennon et al. (1992). A description of the observations and reductions, together with a very useful atlas of Galactic B supergiants can be found there. In Table 1 we list the M33 and Galactic stars used for the present paper.

Equivalent widths for the oxygen and silicon lines were measured by a non-linear least-squares fitting procedure to fit Gaussian profiles to the absorption lines of interest. Blended lines were fitted by multiple Gaussians to estimate the equivalent widths of the individual components. Data and fits were visually inspected and an interactive fit was made to obtain the errors. The estimated errors reflect the range of

equivalent widths deduced using different local continuum levels and the qualitative accuracy of the profile fit. For the Galactic stars we adopted the equivalent widths from Lennon et al. (1993) after checking with some cases that our measurements are consistent with theirs. In this case, the errors were adapted from the qualitative scale given by Lennon et al. (1993) by assuming an error close to the maximum possible error given in Lennon et al. (1993). In a few particular cases we measured it directly from the spectrum, following the same technique as for the M33 stars. Typical errors vary between 10% and 20%, with extreme values at 5% and 30%. The measured equivalent widths and adopted errors are listed in Table 2.

3. Model calculations

For the present paper we have calculated a large number of model atmospheres, including small coarse grids around the T_{eff} values initially assigned to each spectral type. We first generated H/He non-LTE model atmospheres using the ALI code (Kunze (1995)). The models assume plane-parallel geometry with both hydrostatic and radiative equilibrium but metal line-blanketing is omitted. We have adopted a solar helium abundance for all models. Although a few tests we performed showed that the He abundance has an effect on the Si ionization equilibrium, recent results seem to suggest that early B supergiants with low rotational velocities have at most moderate He enrichments (see McErlean et al. (1998b); Smith & Howarth (1998)) and thus we adopted a normal He abundance ($\epsilon = N(\text{He})/(N(\text{H}) + N(\text{He})) = 0.09$). This also agrees with the findings of McErlean et al. (1998a) indicating that spectral analyses of Galactic B supergiants are consistent with moderate or zero He enrichment. Non-LTE line-formation calculations were performed using the codes DETAIL and SURFACE. H and He model atoms have been taken from Herrero et al. (1992). In the calculation of line profiles of H and He, we occasionally had to perform preliminary runs where Lyman lines were set in detailed balance (see below). These populations were used in a second run with the Lyman lines taken fully into account. For the calculations of the metal lines, the atomic data used were taken from Becker & Butler (1988) for O II and Becker & Butler (1990) for Si II/III/IV. Usually the Si III resonance lines were set into detailed balance. Microturbulence has been included in the line formation calculations (i.e., in the statistical equilibrium equations) and in the formal solutions. In all cases, populations were considered converged when they reached relative corrections of 10^{-3} .

Two main assumptions have been made to improve convergence and save computer time whenever possible. First, below 20 000 K, the Lyman series was kept in detailed balance during the calculation of the model atmospheres. This means that we assume that, due to the large optical depth, the upwards radiative rates cancel out the downwards radiative rates exactly, thus allowing the corresponding terms to be analytically deleted from the statistical equilibrium equations. The levels are still connected through collisions and, indirectly, through the continuum. As this approximation could be important for the Si ionization balance used to determine temperatures, we have studied its effect on the equivalent widths of the relevant Si lines. Figure 7 shows the difference between the temperature runs of two models calculated at $T_{\text{eff}} = 22\,500$ K (where the error in setting the Lyman lines in detailed balance will be greater than below 20 000 K), with and without the Lyman series in detailed balance. The formation depth of relevant lines of Si II and Si III are also plotted. We see that the Si II lines are formed much deeper than the zone where the changes

are relevant. This is not the case for the Si III lines, which are stronger and their cores form where the temperature changes begin. However, their equivalent widths vary by less than 5 mÅ, which is largely below our measurement errors. The reason is that at the low densities and high temperatures of the upper layers of early B supergiants, the local temperature is not the only factor determining the populations, and thus small changes in the local temperature have a relatively small influence.

We also show in Figure 7 the populations of $4s\ ^3S^e$, the lower level of Si III $\lambda 4553$ (which we take as representative of the other lines in the triplet), where we see that the changes are only significant in the very upper layers of the atmosphere. In addition, the upper and lower levels of the transition vary in a similar way. Thus the ratio of the departure coefficients, which determines the line source function, remains nearly the same, and the line is only marginally affected.

The second main approximation has been to set the resonance lines of Si III into detailed balance. We begin by discussing the effect at a microturbulence velocity of 0 km s^{-1} . Again, there are variations in the level population which are not large at the depth where the optical Si III lines form (see Figure 7, where we can again see the populations of the lower level of Si III $\lambda 4553$), and therefore the changes in the equivalent widths of these lines are small, of the order of 2–3 mÅ, when the Si III resonance lines are set into detailed balance in the model with $T_{\text{eff}} = 22\,500\text{K}$, $\log g = 2.50$, $\epsilon = 0.09$, independently of the fact that the Lyman lines were or were not set in detailed balance during the model calculations. In Figure 7 we show the ratio of the departure coefficients of the upper and lower levels (these levels are actually a packing of individual levels, see Becker & Butler (1990), but this does not affect our reasoning here) of Si III $\lambda\lambda 4553, 4568, 4574$ with and without the resonance lines of Si III in detailed balance, together with the depth where the line core forms. The small variation of this ratio, which determines the line source functions, means that only the very center of the line varies a little, and thus the effect on the equivalent width is very small (in the example of Figure 7 the difference in the flux is 0.2% in the line center, reaches a maximum of 0.6% at 0.6 Å from line center and disappears at 1 Å from it). The variations of the Si II and Si IV lines are of the same insignificant order.

When we repeat these calculations at $\xi = 15 \text{ km s}^{-1}$ the variations in the equivalent widths are again of only a few mÅ (thus even reducing the percentage change, because the equivalent widths are now larger). The reason is illustrated by Figure 7, where we again see the changes in the population of $4s\ ^3S^e$ when the resonance lines of Si III are set in detailed balance or not. Comparing with Figure 7 we see that the changes in the population of this lower level of Si III $\lambda 4553$ are even lower than for the case with $\xi = 0 \text{ km s}^{-1}$. The increase in the number of absorbing atoms as a consequence of microturbulence makes the approximation of detailed balance even more realistic, as the resonance transitions are now even more opaque. Thus the final equivalent widths are much larger than without microturbulence, but the differences when setting the resonance lines in detailed balance or not remain very small (1–3 mÅ).

In view of the small effects that these approximations introduce, compared with the measurement errors and taking into account that we will perform a differential abundance analysis, we conclude that the approximations made will not have any influence on our results.

4. Parameter determination

Our procedure for determining the stellar parameters is as follows. As Balmer lines are almost unaffected by ξ , H_δ , and H_γ have been used as indicators of $\log g$. For each grid value of T_{eff} we have determined a unique $\log g$, for which observed and theoretical Balmer-line profiles agreed best. In this way, preliminary values of $(T_{\text{eff}}, \log g)$ were first determined. Figure 7 illustrates this for the case of M33 1054.

For each of these $(T_{\text{eff}}, \log g)$ pairs fitting the Balmer lines we calculated silicon line equivalent widths at different ξ . A solar silicon abundance is initially assumed. For each pair of Si lines of two successive ionization stages, a diagram with theoretical equivalent-width ratios is constructed (see Figure 7). We then compare with the observed equivalent width, and interpolate the values of T_{eff} , $\log g$, and ξ that fit this observed equivalent width. The error bars are used to place limits to the determined values of the stellar parameters. This step of the procedure is illustrated in Figure 7, again taken from the analysis of M33 1054. One of these plots is produced for each ratio of Si lines in two successive ionization stages, and the average values of T_{eff} and $\log g$ are adopted.

We then considered the preliminary value of the $(T_{\text{eff}}, \log g)$ pair as fixed and the microturbulence and Si abundance were freely varied in order to ensure that the derived abundances from individual lines were not a function of strength. Si III lines, which come from a single multiplet, were chosen to create the diagram of Si abundance against observed equivalent width. The new values of microturbulence and Si abundance are obtained by demanding a zero slope in the (EW-Abundance) plane of Si III lines, for those abundances compatible with the other ionization stages.

The so defined Si abundance served as a basis for a new $(T_{\text{eff}}, \log g)$ determination. These steps are repeated until the change in T_{eff} , $\log g$, ξ , and Si abundance was within the error in the equivalent-width measurements. This step is also illustrated by Figure 7. From this figure and those corresponding to the other line ratios we can read out the parameters and the error box, which is given by the uncertainty in equivalent widths. Note here that T_{eff} , $\log g$, ξ and Si abundance are determined simultaneously, and there is a unique combination of these four parameters for each point within the error box. Thus not all combinations of stellar parameters are possible and the errors in these quantities are given by the equivalent widths errors. Errors have been adopted by taking the largest error box consistent with all line ratios. Adopted values are $+1000/-800$ K in T_{eff} , ± 0.1 in $\log g$ and ∓ 2 km s $^{-1}$ in ξ . For the Si abundances, we have taken individual abundances for each line and adopted as error the variation of the abundance within the error box. Typical error abundance values oscillate between 0.1 and 0.2 dex.

Table 3 lists the results of our analyses of the M33 B supergiants and their Milky Way comparison standards. We explicitly indicate whether the stellar parameters have been obtained by using the Si III/Si IV or Si II/Si III equilibria, since there are some differences in the results, as can be seen for example in the derived parameters of M33 1054 or in the O abundances of the Galactic stars.

Table 4 gives the errors in the O abundance due to the uncertainties in the equivalent width measurements and in the model parameters for the M33 objects. Note that the situation is different as for the Si abundance, as now the model parameters are independent from the derived O abundance. Thus errors have

been added quadratically. To calculate them we have computed, at different abundances, a fine grid of models around those given in Table 3 as defined by the respective error boxes. We see that final errors are mostly dominated by the uncertainty in equivalent widths. The same procedure has been used for the Galactic comparison stars.

Tables 5 and 6 give the Si and O abundances derived for each individual line used in the study. The average values have been calculated by weighting individual values with the inverse square errors and final errors have been calculated using the quadratic mean of individual errors. We see from the table that individual lines can give quite different values, but no systematic pattern can be appreciated, especially when we consider the behavior of the Galactic standards. This points to the comparatively low S/N ratio of the M33 stars as the main reason for individual variations in the extragalactic sample.

Absolute abundances are listed, but given the present state of the art of B-supergiant model atmospheres, we think that the differential abundances are more trustworthy, and thus we prefer to derive stellar differential abundances from individual differences, following the ideas presented by Smartt et al. (1996). In Tables 7 and 8 we give the differential Si and O abundance between the M33 stars and their Galactic counterparts for each individual line. Again, some individual variations are very large, but we preferred to retain them all in this work because of the small number of available lines. The final adopted differential abundances are given later in § 6. We have retained the individual values for each comparison star.

5. Comments on the spectral analyses

In this section we comment on the individual analyses and the problems found in them. We first consider the analysis of the Galactic stars as a whole, and later we comment on the M33 stars.

Galactic standards The Galactic objects we have analyzed here have been analyzed before by McErlean et al. (1998a) using similar methods. The first thing that is evident when we compare our results with those of McErlean et al. (1998a) is a difference in temperature for some of the stars in common. In Figure 7 we have plotted the temperature scale fitted to the data given by McErlean et al. (1998a) by assigning a number to each spectral type, as well as the values obtained by McErlean et al. (1998a) and ourselves for the stars analyzed here. We see that, for B1.5 and above, the results differ, especially for HD 13 854 and HD 14 956, our temperatures being lower by up to 2 000 K (10 %). Correspondingly, our gravities are lower and our microturbulence velocities higher.

We attribute these difference to our use of the Si III triplet close to 4550 Å, instead of the weaker Si III triplet at $\lambda\lambda$ 4813, 4819, 4829 that was chosen by McErlean et al. (1998a) for their analyses. Of course, our choice is primarily determined by the observations of the extragalactic stars, which, because of observing-time limitations, had to be wavelength restricted.

The main reason why McErlean et al. (1998a) disregarded the bluer triplet lines was that they do not behave as expected. It is expected that their strength increases with decreasing gravity at a fixed temperature,

and, although this is the general trend, for very low gravity models McErlean et al. (1998a) find a filling-in of these lines that they do not consider to be real and attributable to the plane-parallel approximation (which leads to unrealistically low densities in the upper layers of the model atmosphere). The Si III $\lambda\lambda 4813, 4819, 4829$ lines, being weaker, should have a better and more realistic behavior in the plane-parallel models. We agree with the results of McErlean et al. (1998a), although we find a similar, less marked, trend in the Si III $\lambda\lambda 4813, 4819, 4829$ lines.

Given the tests described in the preceding section, we do not consider the approximations made there to be the reason for the temperature differences, but rather that it is to be attributed to the use of two different criteria. Of course, with the limitations of the plane-parallel, hydrostatic models the weaker lines should be preferred, although they are also of more limited application and for the present work, with very faint extragalactic stars, these lines would have had large errors in the equivalent width measurements. The question of which particular criteria are to be preferred can be completely solved only with the use of spherical models with mass-loss, which are more adequate for early B supergiants. Of course, we are implicitly assuming that with a differential analysis such as the one presented here the influence of the particular criteria adopted will only be of secondary importance.

We can also see in Table 6 that the Galactic stars show a trend towards larger O abundances for those stars with parameters determined through the Si III/Si IV ionization equilibrium, as compared to those for which the Si II/Si III equilibrium was used. The difference is large (0.4 dex on average) and the first idea would be to consider that this is related to the above discussion concerning the differences in temperature with McErlean et al. (1998a). Note, however, that the stars for which we obtain the temperature differences with McErlean et al. (1998a) are just those for which the derived O abundance is solar, or close to it, in agreement with what might be expected. This again justifies that comparisons be made in a strictly differential way.

Another peculiarity is the high Si abundance found for HD 14 956, a factor of two larger than the solar abundance. This comes mainly from the low temperature and gravity, which would mean that this star is an extreme supergiant. This is supported by its luminosity class and the strong P Cygni profile displayed in H_{α} (slightly stronger than that displayed by HD 13 854 which is hotter, but has a larger gravity and lower luminosity class). Due to this particularity of HD 14 956 we will always use a second Galactic supergiant when deriving differential abundances for the M33 stars.

M33 1054 The analysis of M33 1054 is particularly difficult, because of the possibility of a multiple spectrum and the weakness of the Si IV and Si II lines. In HST WFPC2 images taken with the F439W filter (cycle 6, P.I. J.K. McCarthy) we can see a cluster of stars at the position of M33 1054. This cluster is dominated by one object that corresponds to the bright star we observed. However, there are two indirect indications of multiplicity. Firstly, the absolute magnitude of the star is very bright for a B2Ib star. Ivanov et al. (1993) give $m_V = 16.6$, which, combined with a mean reddening of $E(B - V) = 0.16$ (Massey et al. (1995)), a true distance modulus of 24.64 (Freedman et al. (1991)), and an R value of 3.1, gives an absolute visual magnitude of $M_V = -8.5$. Even using the lowest value found by Massey et al. (1995) for the M33

reddening, we find $M_V = -8.3$, which is extreme for a B2Ib supergiant, although in view of the large scatter present in the spectral type–absolute magnitude calibrations we do not consider this as a definitive proof.

Secondly, the identification of the Si II doublet is dubious. The observed positions of the Si II doublet lines $\lambda\lambda 4128, 4131$ are 4128.88 and 4132.06 as determined from a double-Gaussian fit. There are no other lines to which these positions could be clearly assigned. This means that the lines seem to be displaced with respect to the laboratory position by 0.81 and 1.17 Å, respectively. This could be interpreted as due to a composite spectrum, especially taking into account the position of M33 1054 (its projected distance to the center of M33 is only 1.0 arcmin). However, we cannot see any other sign of multiplicity in the blue spectrum. In particular, the Si III lines do not show indications of a secondary spectrum (nor does the Si IV $\lambda 4116$ line). This means that any possible contamination should come from a spectral type with strong Si II lines and weak Si III ones, i.e., around A0. We have tried to attribute the Si II lines to such a possible cooler companion and have made some numerical simulations using the Galactic standards from Lennon et al. (1992). We have taken the spectrum of HD 14 899, an A0Ib star, and have combined it with that of HD 206 165, a B2Ib star (we have also used HD 21 291, a B9Ia star, to be sure that the luminosity class would not influence the conclusions). After displacing the spectrum of the A0Ib star, the spectra of the A0 and B2 supergiants were combined in a 1:3 ratio for the blue, and 1:1.6 for the red (the ratios were derived assuming that the observed Si II lines are only due to the possible A0 companion; they correspond to a ratio of the stellar radii of 2:1). We then degraded the resolution and the S/N ratio of the composite spectrum to those of the observed spectrum of M33 1054 and compared them. The same procedure was followed with the spectrum of HD 206 165 separately. In Figure 7 we compare the simulations in the blue and in Figure 7 in the red. In the blue (Figure 7) we see that the apparent displacement of the Si II $\lambda\lambda 4128, 4130$ lines can be reproduced from the spectra of the single blue star, while the Si II lines should have been more conspicuous were they to be attributed to a composite spectrum with the given ratio. In Figure 7 we see that the Si II $\lambda\lambda 6347, 6471$ lines should be apparent, although the spectrum is marginally compatible with the observations due to our low S/N ratio in the red. Here, as in the whole spectrum, the qualitative agreement between the simulations and the observed M33 1054 spectrum is better for the single B2Ib spectrum, although we cannot completely rule out the presence of the A0 star. For example, we also see in the red that the C II $\lambda 6578.03$ line is too strong in the simulated single spectrum. Of course, the spectral ratios could be lower than assumed, but then the blue star dominates the observed spectrum more and more. However, as the degradation of the S/N was made by generating a random array of normally distributed numbers with an appropriate standard deviation, the simulations are not unique results, and thus we must be careful with our conclusions.

We should also point out that the possible presence of an A0Ib star does not improve the situation with respect to the bright magnitude, because it would result in a combined magnitude only 0.3 magnitudes brighter than that of the B supergiant. In addition, the equivalent-width ratio Si II(4128+4131) / Si III(4553+4568+4574) is similar to that of HD 206 165, a B2Ib Galactic supergiant, while the Si IV(4116) / Si III(4553+4568+4574) ratio is only slightly lower than that of HD 13 841, a Galactic B1.5Ib star. An additional indication that M33 1054 is dominated by a single object comes from the work of Massey et al. (1996). 1054 can be identified with their UV source UIT 215, for which they find a spectral type of

B3I, but no signs of multiplicity in the optical spectrum, the UV photometry, or the *HST* images. Thus the observed spectrum of M33 1054 is perfectly compatible with a star slightly hotter than HD 206 165 (B2Ib) and slightly cooler than HD 13 841 (B1.5Ib), except for the displacement of the Si II lines at $\lambda\lambda 4128, 4131$.

Thus if we assume our spectrum of M33 1054 to be dominated by a single object, we can reproduce in many simulations the apparent displacement of the Si II lines, while if we assume it to be at least binary, we would expect the Si II lines to be more conspicuous, or have to give the cool companion a very low surface brightness, thus minimizing its contribution to the combined spectrum.

For all these reasons, we concluded that the analysis of M33 1054 would not be seriously compromised by the presence of a possible companion. However, for safety, we have decided to analyze M33 1054 using the Si II and Si IV lines separately, once comparing with HD 206 265 and using the Si II/Si III ionization balance, and a second time comparing with HD 13 841 and using the Si III/Si IV one. We see in Table 3 that the results are quite similar, not only with regard to the stellar parameters T_{eff} , $\log g$, and ξ , but also with regard to the abundances obtained. This gives us strong confidence in our conclusion that M33 1054 is a slightly metal-enriched blue supergiant, a result similar to that found for this star in Paper II.

The fit to the observed M33 1054 spectrum can be seen in Figure 7, where we have plotted the H, He, Si, and O lines in the given wavelength interval. We show here only the fit with the parameters from the Si II/Si III ionization equilibrium (that with the Si III/Si IV one is comparable). We see that the overall agreement is excellent, except for the O II $\lambda\lambda 4276, 4415, 4417$ lines. The first one is affected by the level setting of the local continuum, and the last two are blended with the strong broad interstellar absorption band at 4428 Å. He I lines generally fit well and do not demand an increase in the helium abundance, although such an effect would be hard to see with the quality of the M33 1054 spectrum.

M33 B133 This is an important object, because it defines the central part of our radial M33 gradient (see next section). In Paper I, we classified the star as B2.5Ia. When determining its T_{eff} during this work we realized that the temperatures obtained were much larger than those corresponding to a B2.5 supergiant. The star is more of a B1.5Ia star (we acknowledge P. Massey here, who already indicated this possibility to us after publication of our Paper I). As a consequence (and also as a cause) we classified the star as a normal-metallicity object, which again evidences the interplay between metallicity and stellar classification. The fact that we found a strong metal deficiency in this star in our analysis of Paper II was already an indication of the problem. Thus we here correct our previous classification, as given above in Table 1 and compare with stars of similar temperature (this is the reason why we analyzed HD 198 478 at the beginning, but did not use it in the final comparisons; nevertheless, we decided to keep it in the tables for future reference).

We first compared it with HD 13 854, a B1Iab star. While we obtained similar values for the stellar parameters T_{eff} , $\log g$, and ξ (see Table 3) the O and Si abundances derived were widely different. M33 B133 was seen to be clearly deficient in O and Si with respect to HD 13 854. The large deficiency lead us to use HD 13 841 (B1.5Ib) also as comparison standard, with comparable results, as can be seen in Table 3. Thus we conclude that M33 B133 is largely deficient in α -elements when compared with stars in the solar neighborhood.

This result is qualitatively similar to that obtained in Paper II, where we compared M33 B133 with the Galactic B supergiant HD 198 478, a B2.5Ia star. However, the differential abundance of O obtained in Paper II (-0.45 dex) was more moderate than that obtained here (-0.65 dex). This is an indication that differential misclassification of the stars can introduce important errors in the differential analysis, and that this is the main disadvantage of the technique used in Paper II.

B38 (ob21–108) This star was not included in our previous papers, but we have included it here because it is an early B-supergiant far away from the center of M33, and thus an appropriate substitute of M33 1354, which could not be analyzed here because the Si ionization balance cannot be used as temperature indicator. It has been classified as B1.5Ia⁺ by Massey et al. (1995). The absence of the Si II doublet at $\lambda\lambda 4128, 4130$ Å indicates a spectral type earlier than B2. The line ratios of Si IV $\lambda 4088$ and the O II features around it point to a B1–B1.5 spectral type. The presence and strength of Si IV $\lambda 4116$ suggests that a B1 spectral type would be more appropriate. Finally, a comparison of Mg II $\lambda 4481$ and the Si III triplet around 4550 Å agrees well with a B1 classification. The red spectrogram shows an emission in H _{α} , which along with the relatively narrow H wings, is consistent with a Ia luminosity class. Our spectral classification for ob21-108, then, is B1Ia, which is consistent with Massey et al. (1995).

The spectral analysis of this star resulted in a lower temperature than in the case of B133 and was comparable to that of 1054 in spite of the earlier spectral type. This is a consequence of a lower gravity and larger microturbulence. The abundances, however, are intermediate between those of 1054 and B133, pointing to a slightly metal-deficient star.

110–A The blue spectrum displayed in Figure 7 is actually a merger of spectra obtained in two different observational runs (described in Herrero et al. (1994) and in Paper I). We first checked the overlapping parts for agreement, as we have used the Si III lines from the first observation with the Si IV lines of the second to derive the stellar parameters from the Si ionization balance, as described in the preceding section. We could not find any variation in the blue spectrum.

This object has a very strong H _{α} emission, indicating the presence of a strong wind (see Figure 7). It is clearly the most extreme object in our small extragalactic sample, with a very low gravity and effective temperature, this last in spite of the relatively early spectral type. This can also be seen in the H _{γ} profile, filled in with emission (see Figure 7). For this reason, only H _{δ} (particularly the wings) was used for the gravity determination. Correspondingly, the derived microturbulence is again very large. The results of the last two objects, 110-A and B38, seem to suggest that the derived microturbulences could in part be due to the presence of strong winds, although this is not reflected by the values obtained for the Galactic stars (see Table 3) and actually cannot be stated before a complete wind analysis is done, which is beyond the scope of this paper.

6. Discussion

In this section we would like to discuss two points: the O and Si abundance gradients in M33 derived from the differential analysis of the Galactic and M33 stars, and the comparison of the results obtained in this paper with those obtained with the more approximate (but much less time-consuming) technique used in Paper II.

The O and Si gradients in M33 Table 9 gives the differential Si and O abundances of M33 stars with respect to their Galactic counterparts (obtained from the data in Tables 7 and 8), as well as the projected distance of each to the center of M33 (in arcmin). Average values and errors have been obtained in the same way as in Section 4.

In Figure 7 we have represented the differential O abundances of the M33 stars versus their projected distance from the center of M33. We have retained both values from Table 9 in the plot to get a feel for the present uncertainty level. We also plot in Figure 7 the O gradient derived by Henry & Howard (1995) from H II regions data (actually, from data obtained by several authors). We see that only B133 departs significantly from the gradient given by Henry & Howard (1995). One could conclude (doing some low-number statistics!) that the stellar data are not inconsistent with the results from H II regions and that although more data are needed, as usually claimed in astrophysics, a first guess could be that B133 is a comparatively low metallicity star for its radial position in M33 (of course, one could also find more exotic explanations). In fact, from the three objects that agree with Henry & Howard (1995) we derive a gradient for the O abundance in M33 of -0.20 ± 0.07 dex kpc $^{-1}$, which coincides with that of Henry & Howard (-0.22 ± 0.04 dex kpc $^{-1}$). Also, including M33 B133 we obtain the same value, with a larger error (-0.19 ± 0.13 dex kpc $^{-1}$). However, without the visual guide provided by the solid line in Figure 7 one would not immediately conclude that there exists a linear gradient in the stellar abundances of the M33 stars, but merely that the star near the center (1054) is much more O rich than those beyond 9 arcmin (about 1.8 kpc at the distance of M33) from the center. Thus, a step function would be equally good for representing the stellar data.

This, of course, is due to our lack of data, but indicates that there are other possibilities, apart from a linear radial gradient. The gradient derived from Henry & Howard (1995) is the final result obtained after combining results from different groups. In Figure 7 we have represented our values (the average values of Table 9 now for clarity) together with those of Vilchez et al. (1988), one of the groups whose data were used by Henry & Howard (1995). The data of Vilchez et al. (1988) are represented relative to the solar value (while our values are relative to Galactic standards). We see there that a steep gradient in the inner regions, combined with a flattening (or even a constant value) beyond 10 arcmin would be also consistent with this particular data combination. Thus we simply conclude that the few stellar data are consistent with any possibility of a larger O abundance in the inner regions of M33 than in regions at around 2 kpc (projected distance) and beyond. Obviously, we need to extend our database.

Figure 7 shows the Si differential abundances in M33 from the data in Table 9. This time we see that the differences between the two individual values corresponding to the same object are larger for the outer

stars, reflecting the largely different Si abundance derived for the Galactic stars HD 14 956 and HD 13 854. In spite of this problem, we see that the trend is the same as for the O data, namely that the star at the center has a much larger Si abundance than the outer objects. This similarity is corroborated in Figure 7, where we have represented the Si and O differential abundances found for the M33 stars. It is obvious that they correlate very well, indicating a common origin, in agreement with our present understanding of chemical stellar and galactic evolution (see for example McWilliam, (1997)).

The good correlation between the O and Si gradients has an added value, as it confirms the large O abundance gradient of M33, much larger than that of the Milky Way (-0.07 dex kpc^{-1} , see Gummersbach et al. (1998) for a list of values), M31 (-0.04 dex kpc^{-1} , see Blair et al. (1981)) or M81 and M101 (with values of -0.06 and -0.11 dex kpc^{-1} respectively, see Henry and Howard (1995)). If finally confirmed (as we still have a very limited number of data points) this points to very interesting questions regarding the physical reason for this difference, and would set important constraints to the galactic chemical evolutionary models.

Comparison with the technique in Paper II In Paper II we used an approximate technique to derive the stellar M33 O gradient, whose results we want to compare with the more detailed analysis carried out here. Although all the details of the technique are explained in Paper II, we give here a short description, for greater ease and better understanding of the differences found.

In Paper II we derived the O abundances of B supergiants in M33 and the Milky Way by first classifying the M33 stars and selecting their Galactic counterparts among the stars observed by Lennon et al. (1992) by requiring that they have the same spectral type and luminosity class. We then adopted a spectral classification–stellar parameters calibration from which T_{eff} was obtained. The gravity was then derived by fitting the wings of H_δ at this fixed temperature. We then assumed that the Galactic B supergiants have solar abundances, and then derived the microturbulence of each star in the Milky Way. This microturbulence was then adopted for the corresponding M33 star, and the O abundance then followed directly by comparing the observed equivalent width of O II 4366 with the appropriate line-formation calculations. This procedure has several important drawbacks: a) there could be a *differential* misclassification in one of the stars; b) there could be a difference in the stellar microturbulence of the M33 and the Galactic star; c) the O abundance of the Galactic star could be different from solar; and d) only one line of O II was used. Each of these points could lead to relative differences in the derived O abundances, introducing systematic errors in the derived radial gradient of M33.

In Figure 7 we have represented the differential O abundance obtained in this work versus the same quantity obtained in Paper II for the three stars in common (1054, B133, and 110–A). We see from the figure that the agreement is good, in spite of the fact that all four possibilities mentioned above have occurred at least once.

The effect of the use of more than one line was investigated by Monteverde (1998), who used the technique from Paper II with two lines instead of one, obtaining differences with the results of Paper II quite similar to those obtained here for 1054 and 110–A. Also, a slightly larger relative abundance than in Paper II

was obtained by Monteverde (1998) for B133. Thus, not only does B133 have the largest deviation from the 1:1 line in Figure 7, but also the particular correction due to the wrong spectral classification is larger than that suggested by the distance from the 1:1 line in Figure 7. We conclude that this is the main inconvenience of the technique used in Paper II, although even this results in corrections that do not change the qualitative picture, especially if a sufficient number of objects can be analyzed at a sufficient number of positions.

7. Conclusions

We have presented non-LTE analyses of four M33 early B-supergiant stars and five Galactic counterparts. The first important conclusion of our analyses is that normal, standard quantitative spectroscopic analyses of blue supergiants in galaxies beyond the Magellanic Clouds are perfectly possible even with 4-m class telescopes. Although, of course, a better resolution and S/N ratio than those used here are highly desirable and easily attainable with 8-m class telescopes.

New spectroscopic observations of B38 (ob21–108) have been presented and the object is classified as B1Ia, in good agreement with previous classifications in the literature. The former classification of B133 (B2.5Ia) has been changed to B1.5Ia. We have shown that M33 1054 is most probably a single object, in spite of the large absolute magnitude found in the literature, very unusual for a B2Ib star.

We have shown that it is possible to set the Ly lines in detailed balance during the calculation of the atmospheric structure without affecting the results, in so far as these are based on photospheric lines formed sufficiently deep in the photosphere. The same conclusion has been reached when setting the Si III resonance lines into detailed balance during the line-formation calculations, i.e., during the joint resolution of radiative-transfer and statistical-equilibrium equations. We have shown that this last approximation is even better suited when a large microturbulent velocity is present.

We found a difference in the derived temperatures of the earlier Galactic stars as compared to those obtained by McErlean et al. (1998a) which we attribute to the different lines used for the temperature derivation. Together with some other facts, such as the apparent correlation of O abundance with the particular Si ionization equilibrium used, we conclude that more work is needed before we can trust the absolute abundances derived, and that strict differential analyses are required to perform abundance comparisons.

We then performed a strict differential analysis by comparing results line by line in M33 and Galactic stars with stellar parameters as similar as possible. Two standards were found for each M33 star, even if this resulted in comparing stars differing a little in their stellar parameters to avoid a particular result having a strong unbalancing influence. From this differential analysis we find that our data are compatible with a radial O gradient in M33, such as that derived from H II regions data by Henry & Howard (1995), although one of the four stars departs from the relation, but also with other possibilities, such as a steep increase in the O abundance in the inner region (at projected distances of less than 9 arcmin from the center of M33), followed by a flat O abundance profile towards the outer parts of M33. Si shows the same pattern, and it is shown that Si and O correlate well, as expected for α -elements.

Clearly, more and better data are needed to take this work further, covering one radial direction in M33 with sufficient spatial resolution. Note that at present all objects at the same projected radial distance from the center in any direction are presented together, in spite of the clear inconveniences of this approximation, because it will immediately add a non-physical scatter to the results. Also, the error bars should be reduced, and for this better observations allowing the use of more lines in the analysis are needed.

The comparison of results obtained here with those of the more approximate technique presented in Paper II suggests that this last can be used if a careful spectral classification at the adequate metallicity is performed.

We warmly acknowledge Stephen Smartt for many ideas, discussions and suggestions during the realization of this work. Neil McErlean and Phil Massey are also acknowledged for their contributions through numerous discussions. Terry Mahoney is acknowledged for carefully reading and correcting the manuscript. Our anonymous referee is acknowledged for her/his criticisms, that improved the scientific value of this paper. AH acknowledges support for this work from the Spanish DGES under project PB97-1438-C02-01 and from the Gobierno Autónomico de Canarias under project PI1999/008. The WHT is operated on the island of La Palma by the RGO in the Spanish Obervatorio del Roque de los Muchachos of the Instituto de Astrofísica de Canarias.

REFERENCES

Becker, S. R., & Butler, K., 1988, A&AS, 201, 232

Becker, S. R., & Butler, K. 1990, A&A, 235, 326

Blair, W.P., Kirshner, R.P., Chevalier, R.A. 1981, ApJ, 254, 50

Freedman, W. L., Wilson, C. D., & Madore, B. F. 1991, ApJ, 372, 455

Gummersbach, C.A., Kaufer, A., Schäfer, D.R., Szeifert, T., Wolf, B. 1998, A&A, 338, 881

Heger, A. 1998, PhD Thesis, Technische Universität München

Henry, R. B. C., & Howard J. B. W. 1995, ApJ, 438, 170

Herrero, A., Corral, L. J., Villamariz, M. R., & Martín, E. L. 1999, A&A, 348, 542

Herrero, A., Kudritzki, R. P., Vílchez, J. M., Kunze, D., Butler, K., & Haser, S. 1992, A&A, 261, 209

Herrero, A., Lennon, D. J., Vilchez, J. M., Kudritzki, R. P., & Humphreys, R. H. 1994, A&A, 287, 885

Humphreys, R. H., & Sandage, A. 1980, ApJS, 44, 319

Ivanov, G. R., Freedman, W. L., & Madore, B. F. 1993, ApJS, 89, 85

Kudritzki, R. P. 1998, in VIII Canary Islands Winter School of Astrophysics, Stellar Astrophysics for the Local Group, ed. A. Aparicio, A. Herrero, & F. Sánchez (Cambridge: Cambridge Univ. Press), p. 149

Kudritzki, R. P., et al. 1999, *A&A*, in press

Kunze, D. 1995, PhD Thesis, Ludwig-Maximillian University Munich

Lennon, D. J. 1997, *A&A*, 317, 871

Lennon, D. J., Dufton, P. L., & Fitzsimmons, A. 1992, *A&AS*, 94, 569

Lennon, D. J., Dufton, P. L., & Fitzsimmons, A. 1993, *A&AS*, 97, 559

McWilliam, A. 1997, *ARA&A*, 35, 503

Maeder, A., & Meynet, G. 2000, *ARA&A*, 38, in press

Maeder, A. 1999, *A&A*, 347, 185

Maeder, A., Grebel, E. K., & Mermilliod, J. C. 1999, *A&A*, 346, 459

Maeder, A., & Zahn, J.-P. 1998, *A&A*, 334, 1000

Massey, P. 1998, in VIII Canary Islands Winter School of Astrophysics, Stellar Astrophysics for the Local Group, ed. A. Aparicio, A. Herrero, & Sánchez (Cambridge: Cambridge Univ. Press), p. 95

Massey, P., Armandroff, T. E., Pyke, R., Patel, K., & Wilson, C. D. 1995, *AJ*, 110, 2715

Massey, P., Bianchi, L., Hutchings, J., & Stecher, T. P. 1996, *ApJ*, 469, 629

McCarthy, J. K., et al. 1997, *ApJ*, 482, 757

McErlean, N. D., Lennon, D. J., & Dufton, P. L. 1998, *A&A*, 329, 613

McErlean, N. D., Lennon, D. J., & Dufton, P. L. 1999, *A&A*, 349, 572

Monteverde, M. I. in ASP Conf. Ser., Vol. 131, II Boulder–Munich Workshop on Properties of hot, luminous stars, ed. I. D. Howarth (San Francisco, ASP), p. 188

Monteverde, M. I., Herrero, A., Lennon, D.J., & Kudritzki, R. P. 1996, *A&A*, 312, 24 (Paper I)

Monteverde, M. I., Herrero, A., Lennon, D. J., & Kudritzki R. P. 1997, *ApJ*, 474, L107 (Paper II)

Puls, J., et al. 1996, *A&A*, 305, 171

Smartt, S. J., Dufton, P. L., & Rolleston, W. R. J. 1996, *A&A*, 310, 123

Smith, K. C., & Howarth, I. D. 1998, *MNRAS*, 299, 1146

Venn, K. A. 1999, *ApJ*, 518, 405

Vilchez, J.M., Pagel, B.E.J., Díaz, A.I., Terlevich, E., Edmunds, M.G., 1988, *MNRAS*, 235, 633

Table 1. M33 Program Stars and Galactic Counterparts.

M33 stars			Galactic stars	
Ident.	Spec. type		HD number	Spec. type
110A	0785	B1 Ia ⁺	HD13854	B1Iab
B38	ob21–108	B1 Ia	HD14956	B1.5Ia
B133	0515	B1.5 Ia	HD13841	B1.5Ib
	1054	B2 Ib	HD206165	B2Ib
			HD198478	B2.5Ia

Note. — M33 stars spectral classification is from Paper I. The identification numbers are from Humphreys & Sandage ((1980), first column) and Ivanov et al. ((1993), second column). Compared with Paper I, B38 is a new object and B133 has been reclassified. The Galactic comparison stars from Lennon et al. ((1992)) are also listed.

Table 2. Equivalent widths of the O and Si lines in M33 stars and Galactic standards.

M33 Star	Si III 4553	Si III 4568	Si III 4574	Si IV 4116	Si II 4128	Si II 4130	O II 4317	O II 4319	O II 4366	O II 4661
0785 – 110A	420±30	300±20	200±20	85±15	85±15	150±22	110±10	205±25
ob21-108 – B38	410±30	370±20	165±20	135±15	140±15	220±20	155±15	150±20
0515 – B133	350±30	210±20	165±20	80±15	65±20	110±20	105±20	...
1054	300±20	270±30	170±20	65±10	70±15	120±20	120±10	100±20	125±15	200±30
Galactic Star										
HD13854	430±30	370±26	225±16	160±11	190±13	210±15	215±15	245±17
HD14956	450±31	405±28	255±18	105±7	155±11	170±25	135±9	165±11
HD13841	380±26	335±24	205±14	80±12	145±11	160±11	160±10	205±15
HD206165	335±23	280±20	145±10	35±10	90±15	110±20	105±8	105±15	122±10	160±10
HD198478	245±17	200±14	135±9	...	120±8	160±11	75±18	60±15	60±15	70±15

Table 3. Non-LTE Atmospheric Parameters for the Program Stars.

M33 star		T_{eff}	$\log g$	ξ	Ion. balance	$12 + \log(\text{Si}/\text{H})$	$12 + \log(\text{O}/\text{H})$
110A	0785	19000	2.20	19	Si III/Si IV	7.32 ± 0.15	8.55 ± 0.17
B38	ob21-108	20700	2.37	20	Si III/Si IV	7.24 ± 0.12	8.55 ± 0.13
B133	0515	21300	2.53	15	Si III/Si IV	7.04 ± 0.15	8.22 ± 0.20
	1054	20500	2.50	9	Si III/Si IV	7.61 ± 0.18	8.90 ± 0.22
	1054	21000	2.55	9	Si II/Si III	7.54 ± 0.14	8.79 ± 0.20
Galactic star							
HD13854		21700	2.52	14	Si III/Si IV	7.59 ± 0.11	9.00 ± 0.13
HD14956		19300	2.28	15	Si III/Si IV	7.91 ± 0.13	8.85 ± 0.16
HD13841		21000	2.60	15	Si III/Si IV	7.47 ± 0.12	8.81 ± 0.12
HD206165		20000	2.45	15	Si II/Si III	7.29 ± 0.09	8.59 ± 0.14
HD198478		18500	2.20	8	Si II/Si III	7.55 ± 0.09	8.41 ± 0.29

Note. — Atmospheric parameters have been derived from the silicon ionization balance. Typical errors are ± 1000 K for T_{eff} , ± 0.1 dex for $\log g$, and ± 2 km s $^{-1}$ for ξ . The two lines for 1054 give the two results for the different ionization balance used.

Table 4. O abundance errors of the program stars.

O II line		110A	B38	B133	1054 cool	1054 hot	HD13854	HD14956	HD13841	HD206165	HD198478
4317	model A	0.08	0.03	0.06	0.06	0.05	0.05	0.08	0.08	0.09	0.05
	model B	0.10	0.06	0.07	0.08	0.09	0.07	0.08	-0.02	0.09	0.11
	model C	-0.02	-0.06	-0.06	-0.04	-0.03	-0.04	-0.10	-0.09	-0.09	-0.06
	model D	-0.04	-0.06	-0.08	-0.08	-0.07	-0.06	-0.11	-0.11	-0.09	-0.10
	ΔEW	± 0.15	± 0.10	± 0.24	± 0.15	± 0.10	± 0.10	± 0.09	± 0.08	± 0.07	± 0.30
	Adopted	± 0.17	± 0.12	± 0.25	± 0.17	± 0.13	± 0.12	± 0.13	$\substack{+0.11 \\ -0.14}$	± 0.11	± 0.32
4319	model A	0.09	0.03	0.06	0.06	0.04	0.05	0.09	0.07	0.09	0.06
	model B	0.10	0.06	0.07	0.09	0.08	0.06	0.08	-0.01	0.09	0.10
	model C	-0.03	-0.06	-0.06	-0.04	-0.04	-0.04	-0.09	-0.08	-0.09	-0.06
	model D	-0.04	-0.07	-0.08	-0.07	-0.08	-0.07	-0.10	-0.09	-0.09	-0.10
	ΔEW	± 0.16	± 0.11	± 0.15	± 0.25	± 0.20	± 0.10	± 0.20	± 0.08	± 0.14	± 0.26
	Adopted	$\substack{+0.19 \\ -0.16}$	± 0.13	± 0.17	± 0.27	± 0.22	± 0.12	± 0.22	± 0.12	± 0.17	± 0.28
4366	model A	0.08	0.03	0.02	0.03	0.01	0.03	0.06	0.05	0.05	0.04
	model B	0.10	0.07	0.03	0.08	0.07	0.06	0.07	-0.01	0.06	0.11
	model C	-0.02	-0.05	-0.09	-0.03	-0.03	-0.04	-0.09	-0.07	-0.09	-0.02
	model D	-0.04	-0.07	-0.10	-0.08	-0.08	-0.07	-0.10	-0.09	-0.10	-0.09
	ΔEW	± 0.12	± 0.10	± 0.15	± 0.15	± 0.15	± 0.10	± 0.08	± 0.07	± 0.08	± 0.26
	Adopted	$\substack{+0.16 \\ -0.13}$	± 0.12	$\substack{+0.15 \\ -0.18}$	± 0.17	± 0.17	± 0.12	± 0.12	± 0.10	$\substack{+0.10 \\ -0.13}$	± 0.28
4661	model A	0.10	0.04	0.06	0.06	0.05	0.04	0.09	0.06	0.10	0.06
	model B	0.12	0.08	0.08	0.08	0.10	0.07	0.09	-0.01	0.09	0.11
	model C	-0.03	-0.06	-0.06	-0.04	-0.02	-0.05	-0.11	-0.08	-0.09	-0.07
	model D	-0.05	-0.08	-0.08	-0.08	-0.07	-0.08	-0.11	-0.09	-0.10	-0.11
	ΔEW	± 0.15	± 0.13	...	± 0.25	± 0.24	± 0.11	± 0.08	± 0.10	± 0.08	± 0.24
	Adopted	$\substack{+0.19 \\ -0.16}$	± 0.15	...	± 0.26	± 0.26	± 0.14	± 0.13	± 0.13	± 0.26	

Note. — Uncertainties in the O II abundance determinations. Models A, B, C, D refer to models calculated with the parameters from Table 3 and the following parameter shifts in T_{eff} , $\log g$ and ξ , respectively: model A, (+1000 K, +0.1 dex, -2 km s $^{-1}$); model B, (+500 K, +0.05 dex, 0 km s $^{-1}$); model C, (-800 K, -0.08 dex, +2 km s $^{-1}$); model D, (-500 K, -0.05 dex, 0 km s $^{-1}$). ΔEW refers to the uncertainty caused by the equivalent width error measurements. Uncertainties have been added quadratically to give the adopted errors. Cool and hot models of 1054 refer to the results obtained with the Si III/Si IV and Si II/Si III ionization equilibria respectively

Table 5. Silicon abundances of the Program Stars.

M33 star		Si III 4553	Si III 4568	Si III 4574	Si IV 4116	Si II 4128	Si II 4130	12 + log(Si/H)
110A	0785	7.36±0.11	7.19±0.08	7.42±0.11	7.33±0.21	7.32±0.15
B38	ob21-108	7.15±0.10	7.31±0.08	7.17±0.10	7.14±0.15	7.24±0.12
B133	0515	7.15±0.13	6.80±0.10	7.18±0.12	7.07±0.22	7.04±0.15
	1054	7.58±0.15	7.68±0.20	7.61±0.15	7.57±0.20	7.61±0.18
	1054	7.52±0.13	7.61±0.18	7.55±0.15	...	7.50±0.10	7.64±0.10	7.54±0.14
Galactic Star								
HD13854		7.54±0.12	7.57±0.11	7.54±0.10	7.68±0.11	7.59±0.11
HD14956		7.85±0.15	7.96±0.14	7.90±0.11	7.91±0.09	7.91±0.13
HD13841		7.40±0.11	7.48±0.11	7.48±0.08	7.53±0.18	7.47±0.12
HD206165		7.29±0.11	7.31±0.10	7.18±0.07	...	7.38±0.06	7.32±0.07	7.29±0.09
HD198478		7.57±0.13	7.50±0.12	7.58±0.09	...	7.53±0.05	7.58±0.06	7.55±0.09

Note. — Silicon abundances are derived from each particular line. The last column gives the stellar abundance. The first line of M33 1054 gives the results for the Si III/Si IV ionization balance, and the second line gives the results for the Si II/Si III ionization balance.

Table 6. Oxygen Abundances of the Program Stars.

M33 star	O II	O II	O II	O II	12 + log(O/H)
	4317	4319	4366	4661	
110A	0785	8.24±0.17	8.70 ^{+0.19} _{-0.16}	8.36 ^{+0.16} _{-0.13}	8.97 ^{+0.19} _{-0.16}
B38	ob21-108	8.47±0.12	8.89±0.13	8.46±0.12	8.38±0.15
B133	0515	7.96±0.25	8.34±0.17	8.22±0.18	...
	1054	8.89±0.17	8.59±0.27	8.80±0.17	9.43±0.26
	1054	8.79±0.17	8.52±0.22	8.71±0.17	9.33±0.26
Galactic Star					
HD13854		8.92±0.12	9.00±0.12	8.94±0.12	9.21±0.14
HD14956		8.96±0.13	9.03±0.22	8.65±0.12	8.92±0.13
HD13841		8.74 ^{+0.11} _{-0.14}	8.81±0.11	8.72±0.10	9.05±0.13
HD206165		8.51±0.11	8.46±0.17	8.52 ^{+0.10} _{-0.13}	8.85±0.13
HD198478		8.63±0.32	8.34±0.28	8.25±0.28	8.45±0.26

Note. — Oxygen abundances are derived from each particular line. The last column gives the stellar abundance. The first line of M33 1054 gives the results for the Si III/Si IV ionization balance, and the second line gives the results for the Si II/Si III ionization balance.

Table 7. Silicon Differential Abundances of the Program Stars.

M33 star		Galactic Standard	Si III 4553	Si III 4568	Si III 4574	Si IV 4116	Si II 4128	Si II 4130
110A	0785	HD13854	−0.18±0.16	−0.38±0.14	−0.12±0.15	−0.35±0.24
		HD14956	−0.49±0.18	−0.77±0.16	−0.48±0.15	−0.58±0.23
B38	ob21-108	HD13854	−0.39±0.16	−0.26±0.16	−0.37±0.15	−0.54±0.17
		HD14956	−0.70±0.18	−0.65±0.16	−0.73±0.15	−0.77±0.17
B133	0515	HD13854	−0.39±0.18	−0.77±0.15	−0.37±0.15	−0.61±0.25
		HD13841	−0.25±0.17	−0.68±0.15	−0.30±0.14	−0.46±0.28
	1054	HD13841	+0.18±0.18	+0.20±0.23	+0.13±0.17	0.04±0.25
		HD206165	+0.23±0.17	+0.30±0.20	+0.37±0.16	...	+0.12±0.11	+0.32±0.12

Note. — Silicon differential abundances are derived from each particular line. The first line of M33 1054 gives the results for the Si III/Si IV ionization balance, and the second line gives the results for the Si II/Si III ionization balance.

Table 8. Oxygen Differential Abundances of the Program Stars.

M33 star		Galactic Standard	O II 4317	O II 4319	O II 4366	O II 4661
110A	0785	HD13854	-0.68 ± 0.21	$-0.30^{+0.22}_{-0.20}$	$-0.58^{+0.20}_{-0.18}$	$-0.22^{+0.24}_{-0.21}$
		HD14956	-0.72 ± 0.21	$-0.33^{+0.29}_{-0.27}$	$-0.29^{+0.20}_{-0.18}$	$+0.05^{+0.23}_{-0.21}$
B38	ob21-108	HD13854	-0.45 ± 0.17	-0.11 ± 0.18	-0.48 ± 0.17	-0.83 ± 0.21
		HD14956	-0.49 ± 0.18	-0.14 ± 0.26	-0.19 ± 0.17	-0.54 ± 0.21
B133	0515	HD13854	-0.96 ± 0.28	-0.66 ± 0.21	-0.72 ± 0.22	...
		HD13841	$-0.78^{+0.27}_{-0.29}$	-0.47 ± 0.20	-0.50 ± 0.21	...
	1054	HD13841	$+0.15^{+0.20}_{-0.22}$	-0.22 ± 0.29	$+0.08 \pm 0.20$	$+0.38 \pm 0.29$
		HD206165	$+0.28 \pm 0.20$	$+0.06 \pm 0.28$	$+0.19 \pm 0.21$	$+0.48 \pm 0.29$

Note. — Oxygen differential abundances are derived from each particular line. The first line of M33 1054 gives the results for the Si III/Si IV ionization balance, and the second line gives the results for the Si II/Si III ionization balance

Table 9. Si and O Non-LTE Differential Abundances.

M33 star	ρ	Standard	$\log(\text{Si}/\text{H})_{\text{M33}} - \log(\text{Si}/\text{H})_{\text{Gal}}$	$\log(\text{O}/\text{H})_{\text{M33}} - \log(\text{O}/\text{H})_{\text{Gal}}$
1054	1'.0	HD206165	+0.25±0.16	+0.25±0.25
		HD13841	+0.14±0.21	+0.18±0.25
		Average	+0.20±0.19	+0.22±0.25
B133	9'.4	HD13854	-0.53±0.19	-0.75±0.24
		HD13841	-0.42±0.19	-0.55±0.24
		Average	-0.48±0.19	-0.65±0.24
ob21-108	11'.7	HD14956	-0.71±0.17	-0.35±0.21
		HD13854	-0.39±0.16	-0.44±0.18
		Average	-0.54±0.17	-0.40±0.20
110A	17'.1	HD14956	-0.58±0.18	-0.33±0.23
		HD13854	-0.25±0.18	-0.47±0.21
		Average	-0.41±0.18	-0.41±0.22

Note. — Silicon and oxygen non-LTE differential abundances for the M33 B supergiants compared to Galactic standards. ρ is the galactocentric distance in arcminutes.

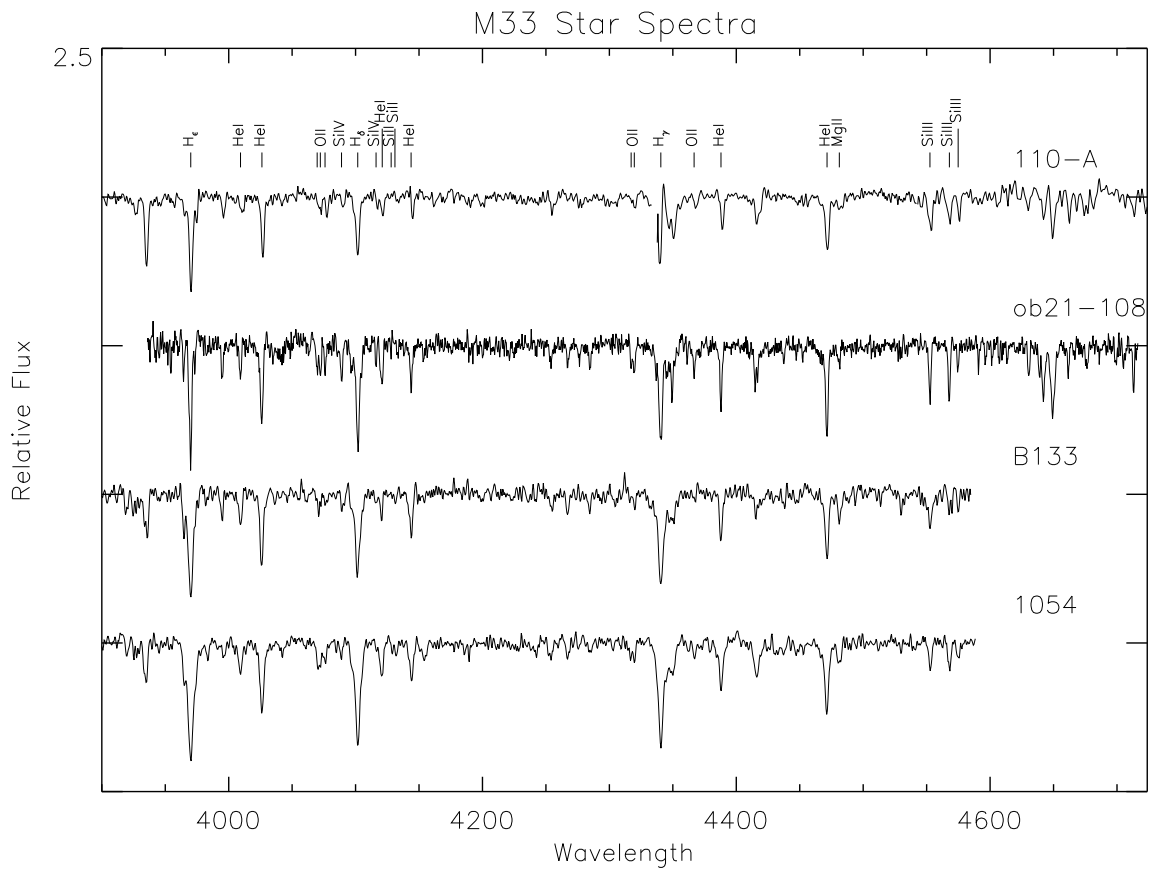


Fig. 1.— Blue spectra of the M33 stars analyzed here, with the most important lines for this paper marked. The spectrum for 110-A is a merging of two different observing campaigns, described in Herrero et al. (1994). The gap in the blue wing of H_{γ} in this star is due to a cosmic ray.

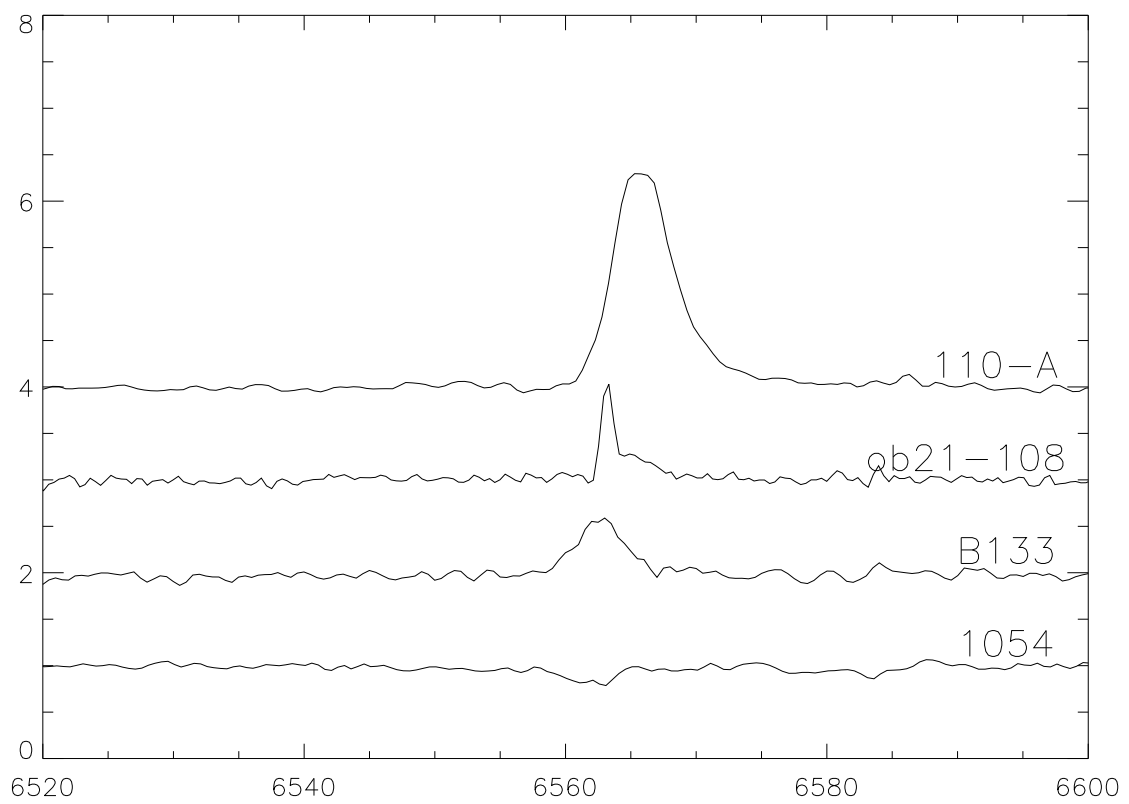


Fig. 2.— H_α spectra of the M33 stars analyzed here.

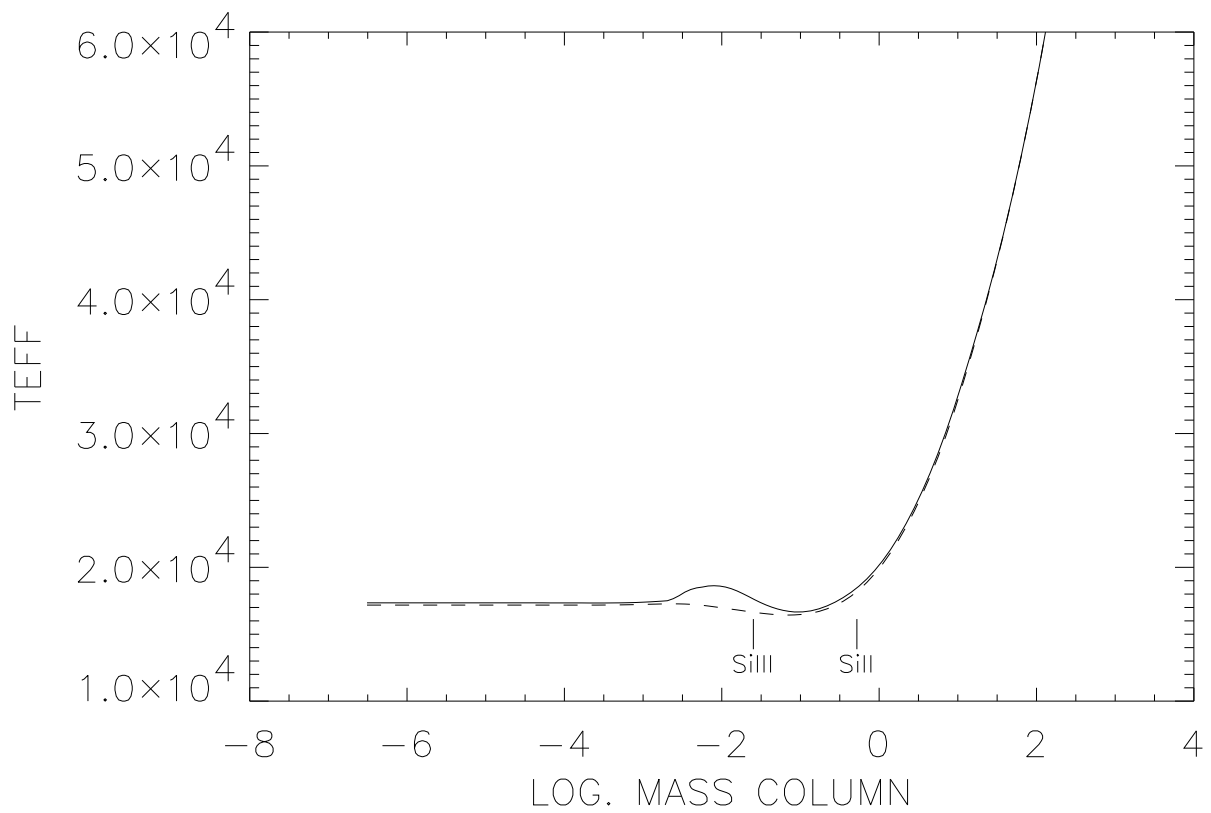


Fig. 3.— Comparison of the temperature runs of two models at $T_{\text{eff}} = 22\,500\text{K}$, $\log g = 2.50$, $\epsilon = 0.09$, with the Lyman lines in detailed balance (dashed line) and not in detailed balance (solid line) during the model atmosphere calculations.

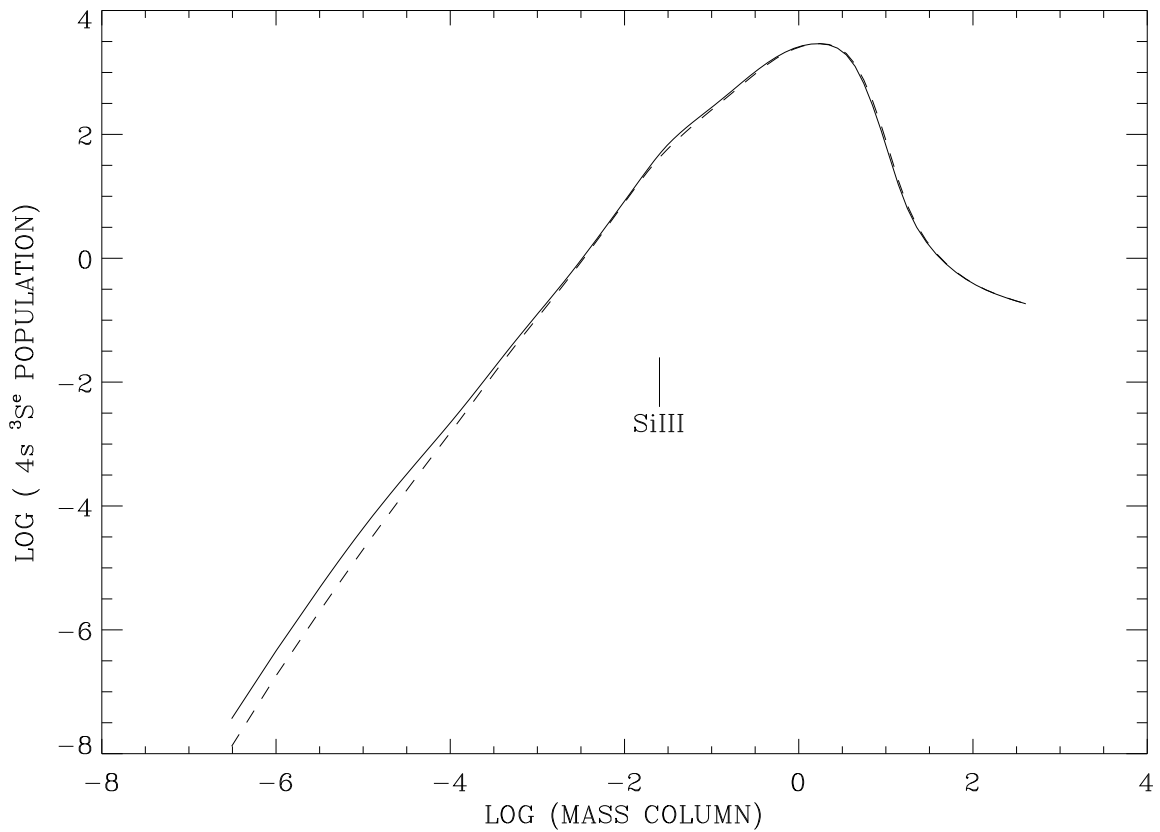


Fig. 4.— Comparison of the populations of $4s\ ^3S^e$, the lower level of Si III $\lambda 4553$, in two models at $T_{\text{eff}} = 22\,500\text{K}$, $\log g = 2.50$, $\epsilon = 0.09$, with the Lyman lines in detailed balance (dashed line) and not in detailed balance (solid line) during the model atmosphere calculations. The formation depth of the line core is also marked. Mass column is given in g cm^{-2} and populations in atoms cm^{-3} .

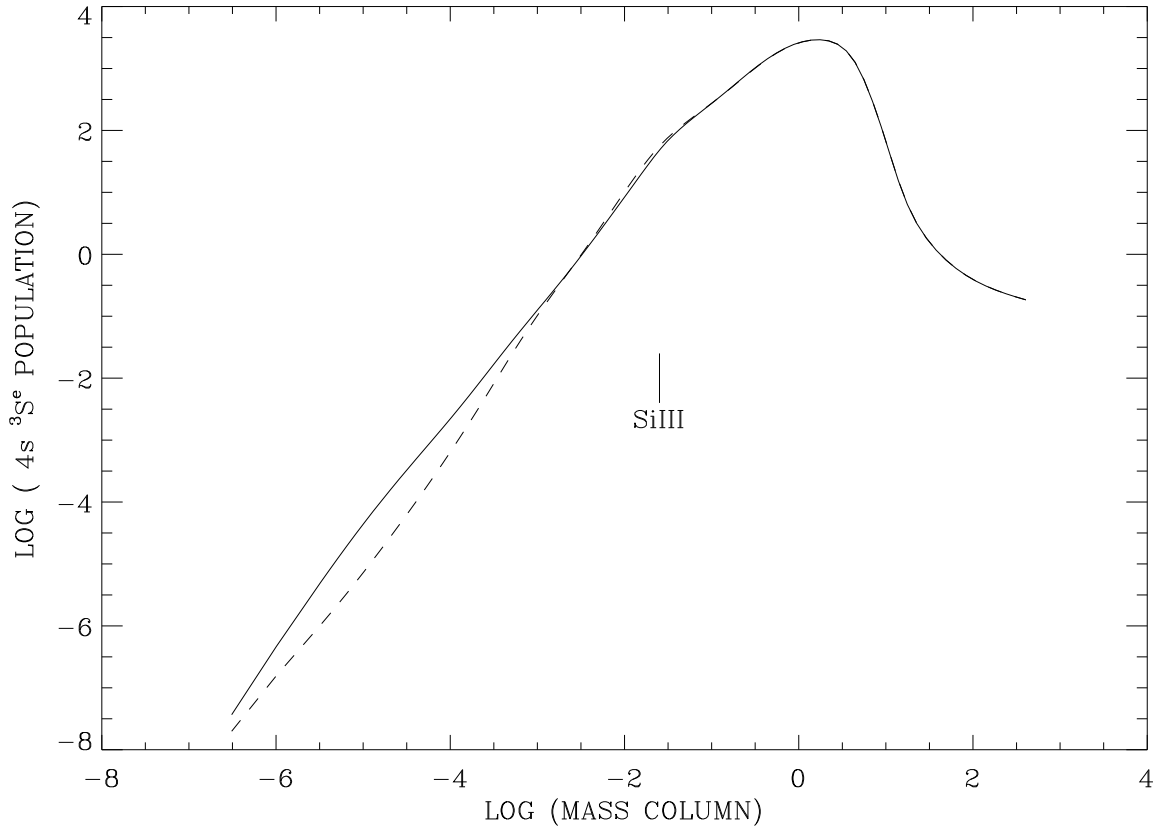


Fig. 5.— Comparison of the populations of $4s\ 3S^e$, the lower level of Si III $\lambda 4553$, in two models at $T_{\text{eff}} = 22\,500\text{K}$, $\log g = 2.50$, $\epsilon = 0.09$, with the Si III resonance lines in detailed balance (dashed line) and not in detailed balance (solid line) during the line formation calculations, with no microturbulent velocity. The formation depth of the line core is also marked. Mass column is given in g cm^{-2} and populations in atoms cm^{-3} .

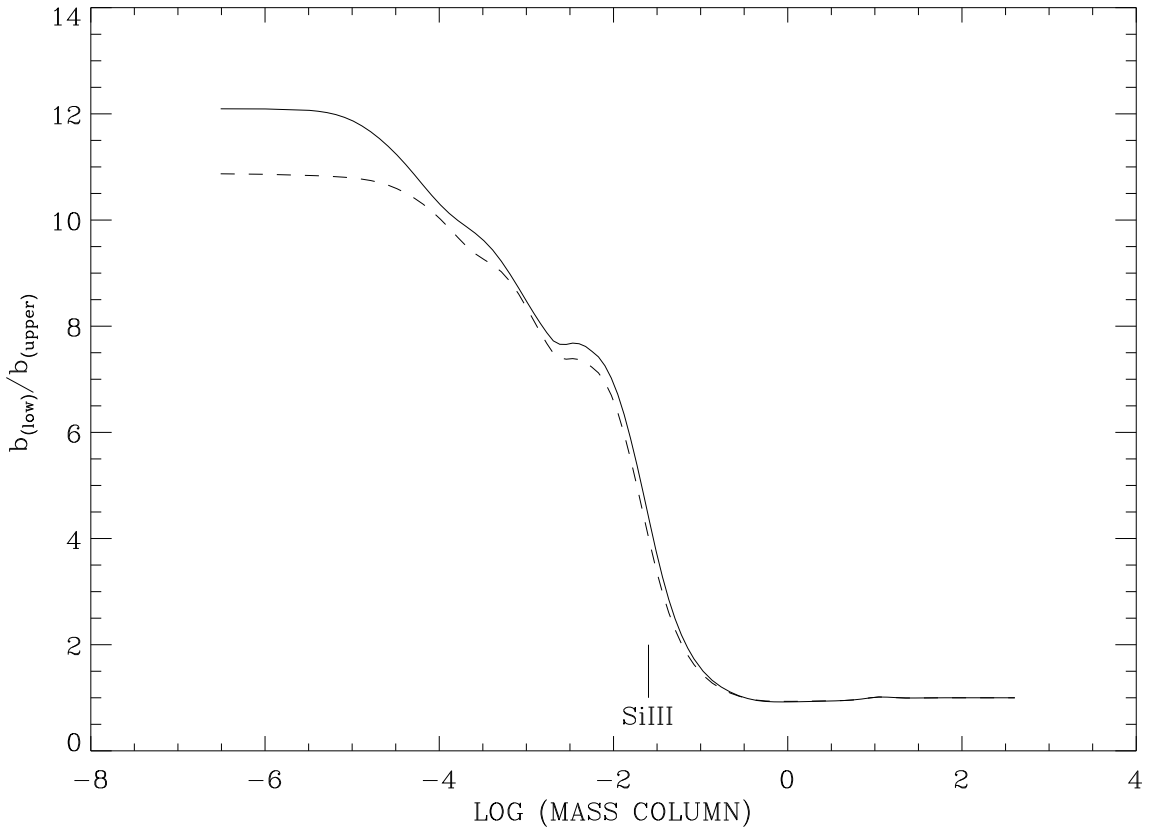


Fig. 6.— Comparison of the ratio of the departure coefficients of $4s\ 3S^e$ and $4p\ 3P^o$, the lower and upper levels of Si III $\lambda\lambda 4553, 4568, 4574$ in two models at $T_{\text{eff}} = 22\,500\text{K}$, $\log g = 2.50$, $\epsilon = 0.09$, with the Si III resonance lines in detailed balance (dashed line) and not in detailed balance (solid line) during the line formation calculations. The formation depth of the line cores is also marked. Mass column is given in g cm^{-2} . Note that this time the vertical axis is not logarithmic as in the previous figures.

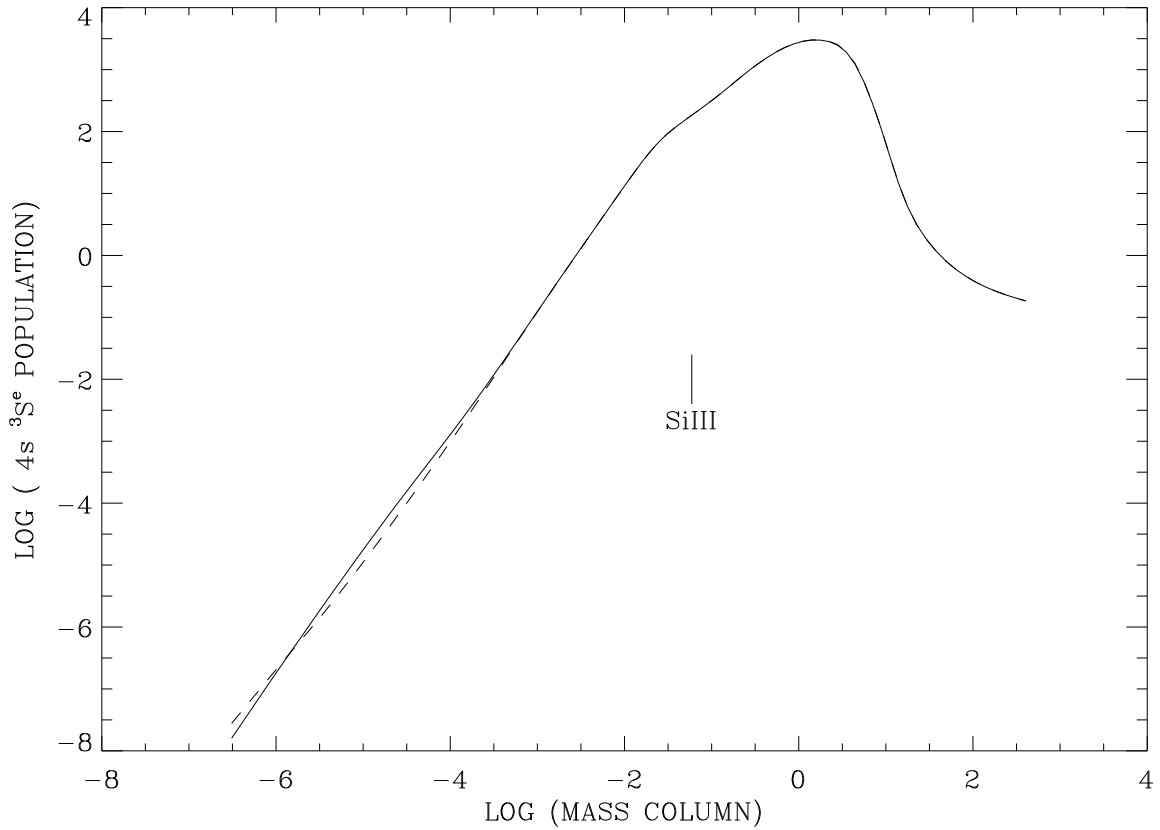


Fig. 7.— Comparison of the populations of $4s\ ^3S^e$, the lower level of Si III $\lambda 4553$, in two models at $T_{\text{eff}} = 22\,500\text{K}$, $\log g = 2.50$, $\epsilon = 0.09$, with the Si III resonance lines in detailed balance (dashed line) and not in detailed balance (solid line) during the line formation calculations, with a microturbulent velocity of 15 km s^{-1} . Compare with Figure 5 where no microturbulence was included. The formation depth of the line core is also marked. Mass column is given in g cm^{-2} and populations in atoms cm^{-3} .

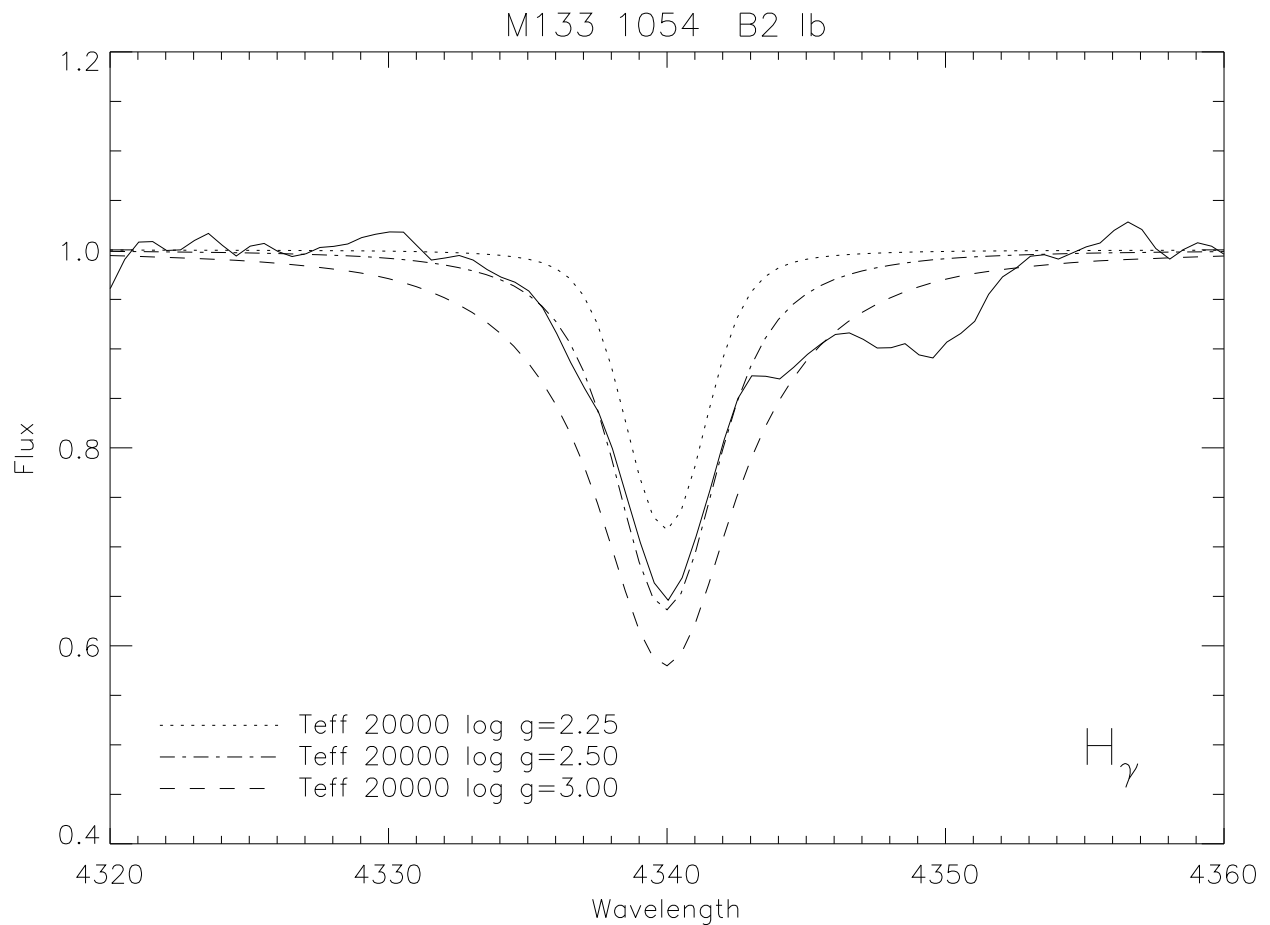


Fig. 8.— The determination of gravity at $T_{\text{eff}} = 20\,000\text{K}$ in M33 1054 using the wings of H_{γ} . The same procedure is used to determine it at other temperatures, giving possible pairs of $(T_{\text{eff}}, \log g)$.

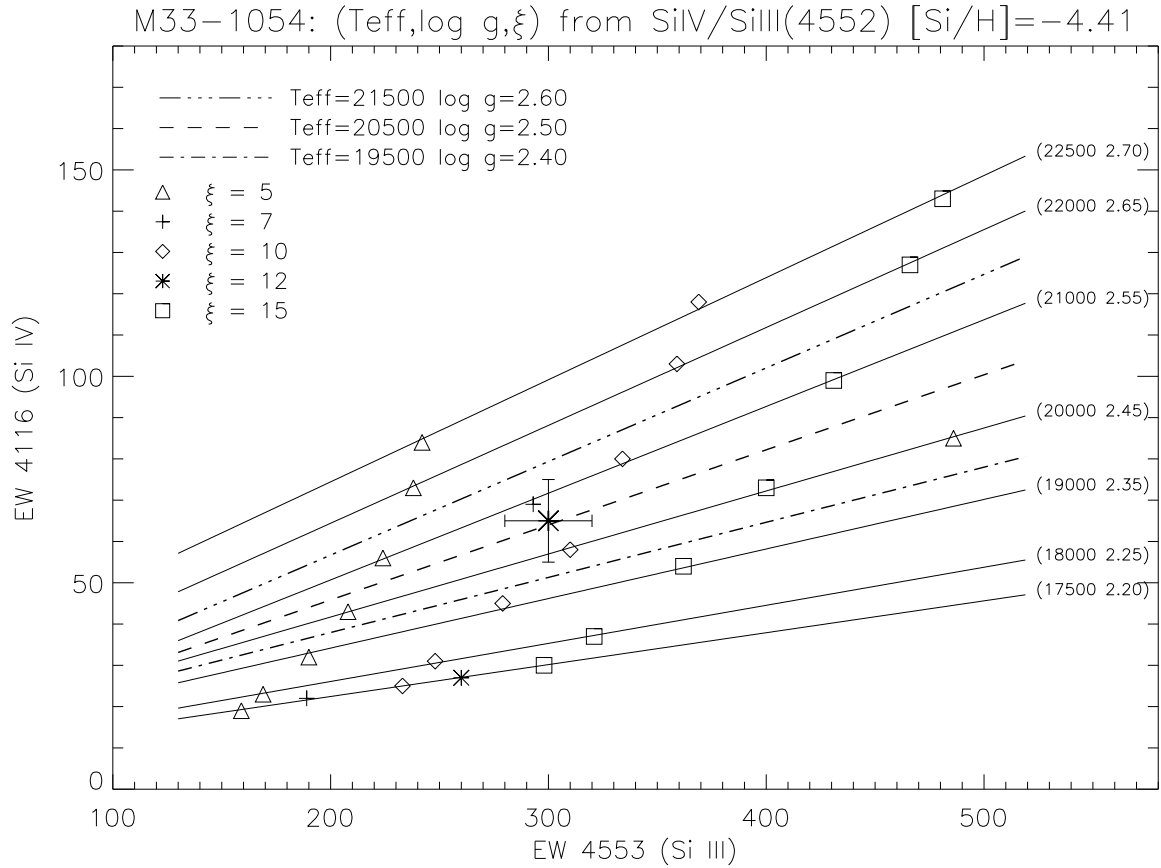


Fig. 9.— Joint determination of microturbulence, T_{eff} and $\log g$ at solar Si abundance for Si III $\lambda 4553$ and Si IV $\lambda 4116$. The possible pairs of T_{eff} and $\log g$ were fixed by the Balmer lines wings. Solid lines indicate models that were explicitly calculated. Different symbols are used for different microturbulent velocities, as indicated in the figure (values are given in km s^{-1}). The cross marks the observed equivalent width. The dashed, dash-dotted and dash-double dotted lines have been obtained by interpolation and give, respectively, the model parameters that fit the observed equivalent width and their adopted upper and lower limits. Similar diagrams are obtained for other pairs of Si lines, to finally obtain a value for T_{eff} , $\log g$, and ξ at the assumed Si abundance.

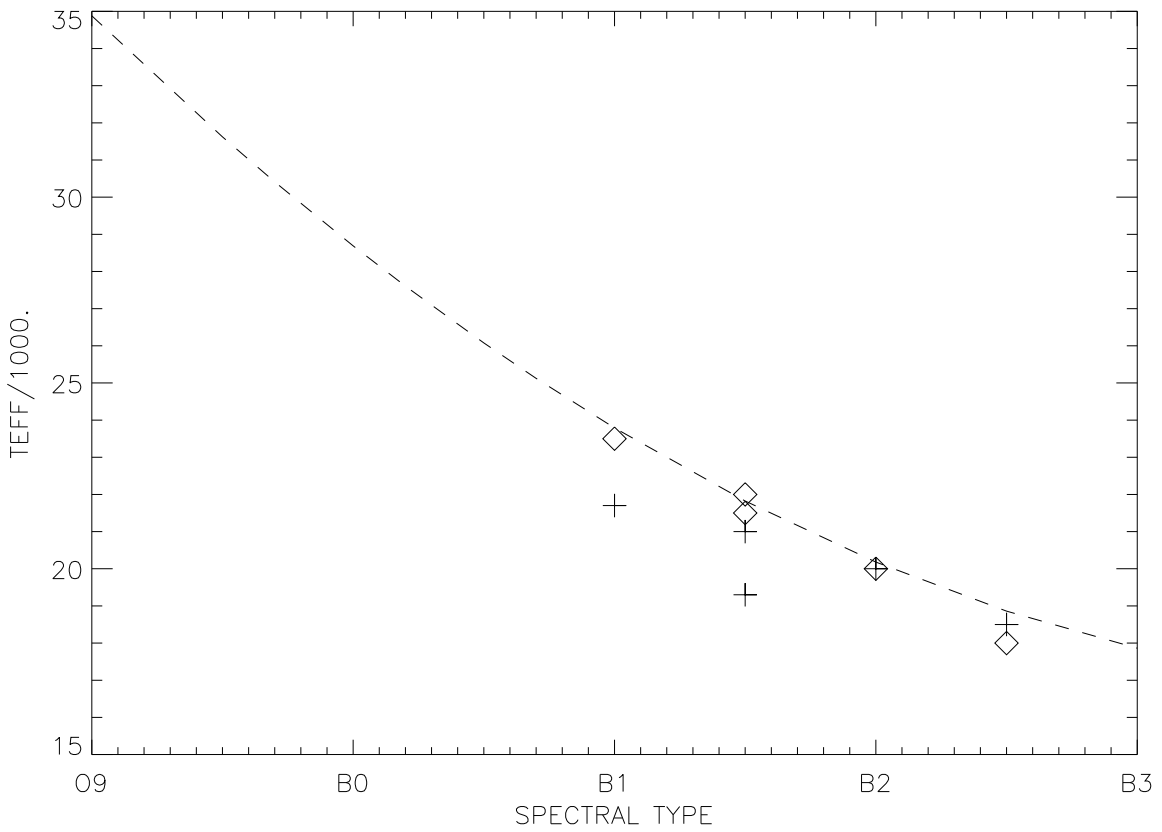


Fig. 10.— The temperature scale for B supergiants from the fit to the data by McErlean et al. (1998a). Diamonds represent the individual values obtained by McErlean et al. (1988a) for the Galactic stars analyzed here, and crosses represent the values obtained in the present work for the same objects.

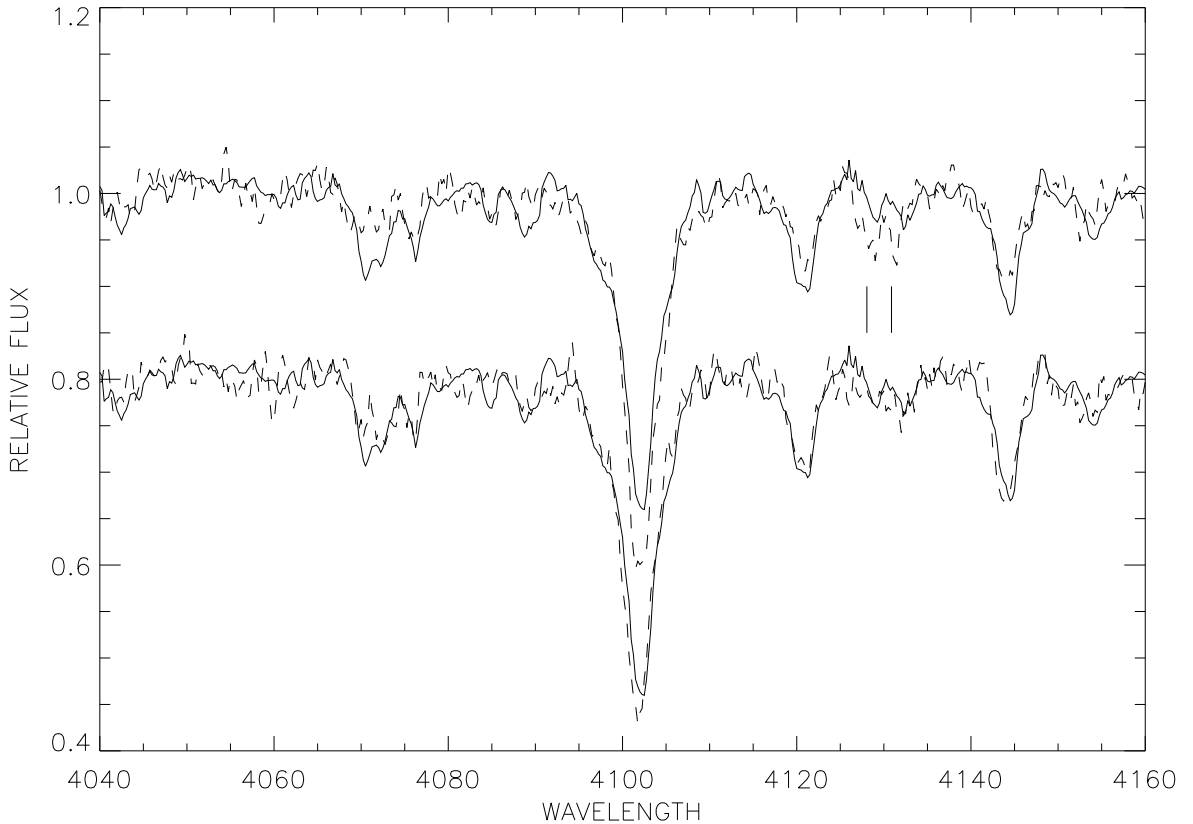


Fig. 11.— Comparison of a portion of the blue spectrum of M33 1054 (solid line) with the simulations of a (B2Ib+A0Ib) binary (dashed line, above) and a single B2Ib star (dashed line, displaced 0.2 to the bottom for clarity). The vertical lines between the spectra mark the laboratory positions of Si II $\lambda\lambda$ 4128, 4130. We see that the simulated binary has more conspicuous Si II lines, and that the single B2Ib star can simulate the apparent displacement of these lines because of noise and low S/N.

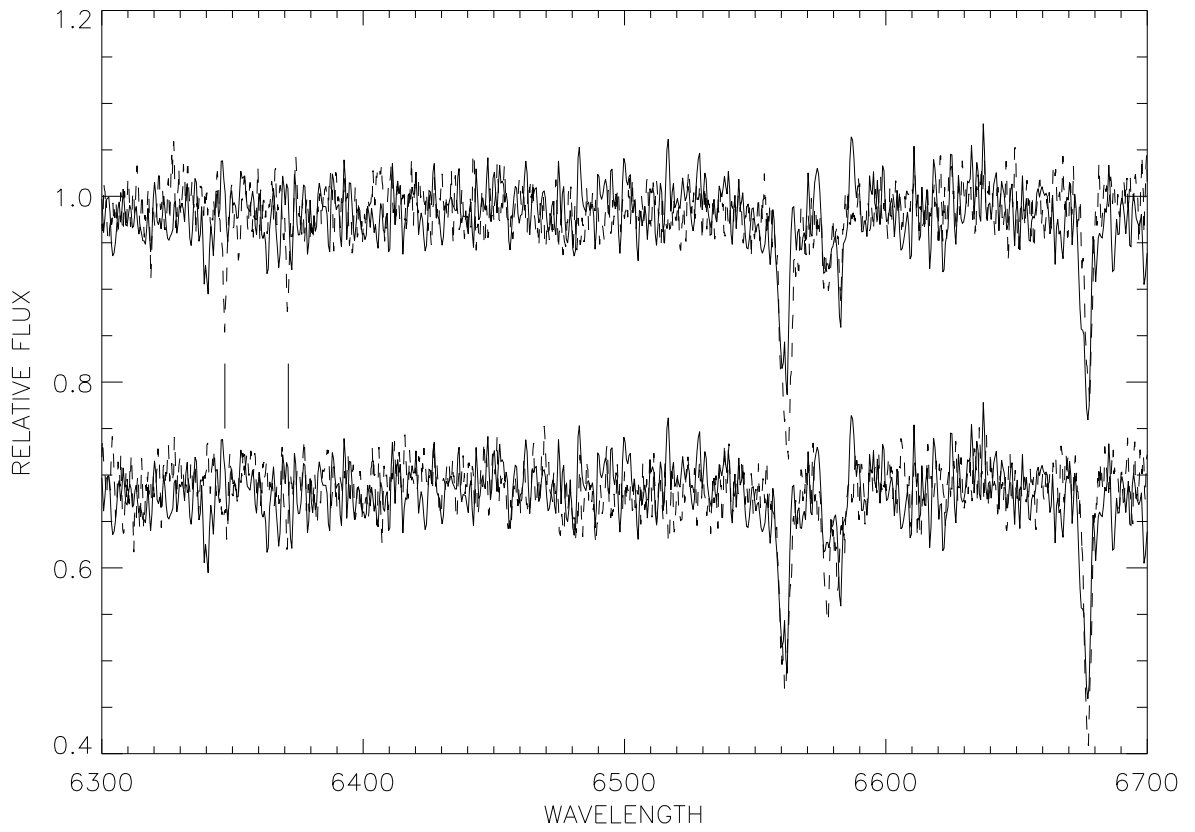


Fig. 12.— Comparison of a portion of the red spectrum of M33 1054 (solid line) with the simulations of a (B2Ib+A0Ib) binary (dashed line, above) and a single B2Ib star (dashed line, displaced 0.3 to the bottom for clarity). The vertical lines between the spectra mark the laboratory positions of Si II $\lambda\lambda$ 6347, 6371. We would expect to see the strong Si II lines if M33 1054 were actually a binary of the assumed characteristics.

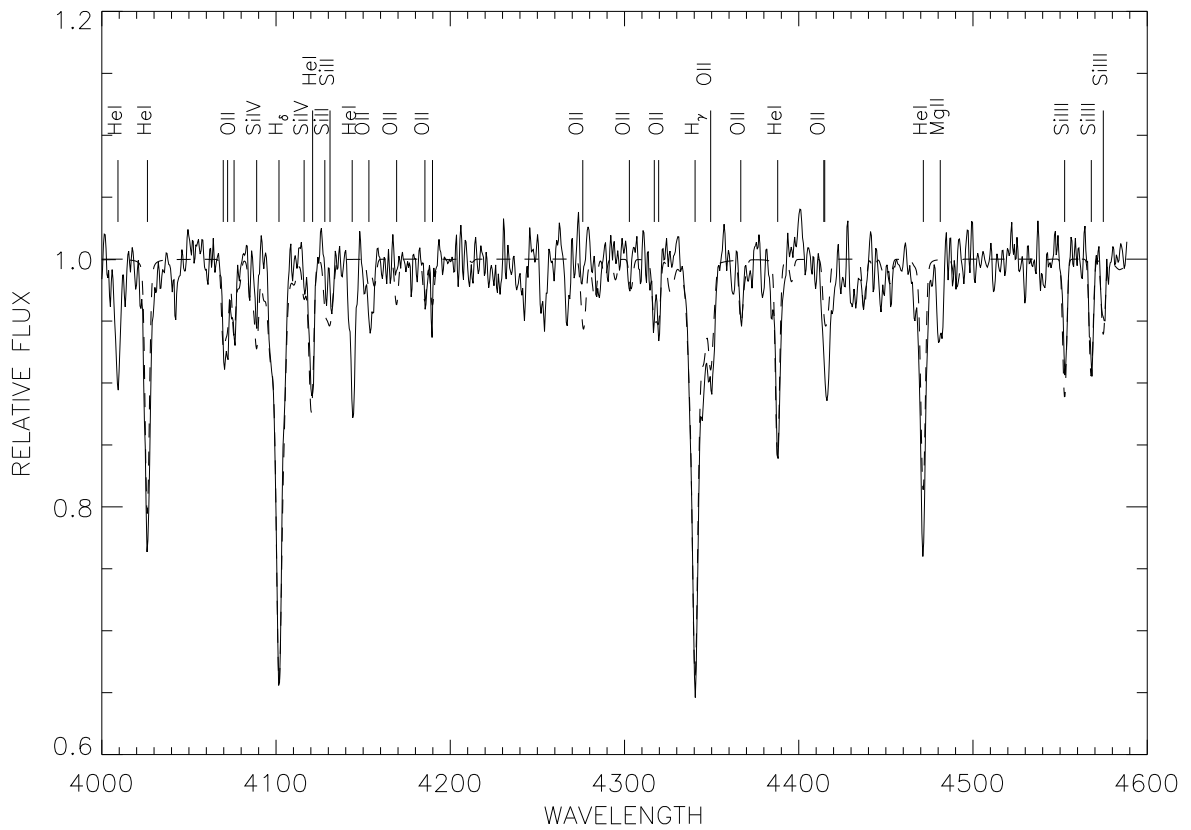


Fig. 13.— The fit to the observed spectrum of M33 1054. We have marked the same lines as in Figure 1 and also those calculated with SURFACE.

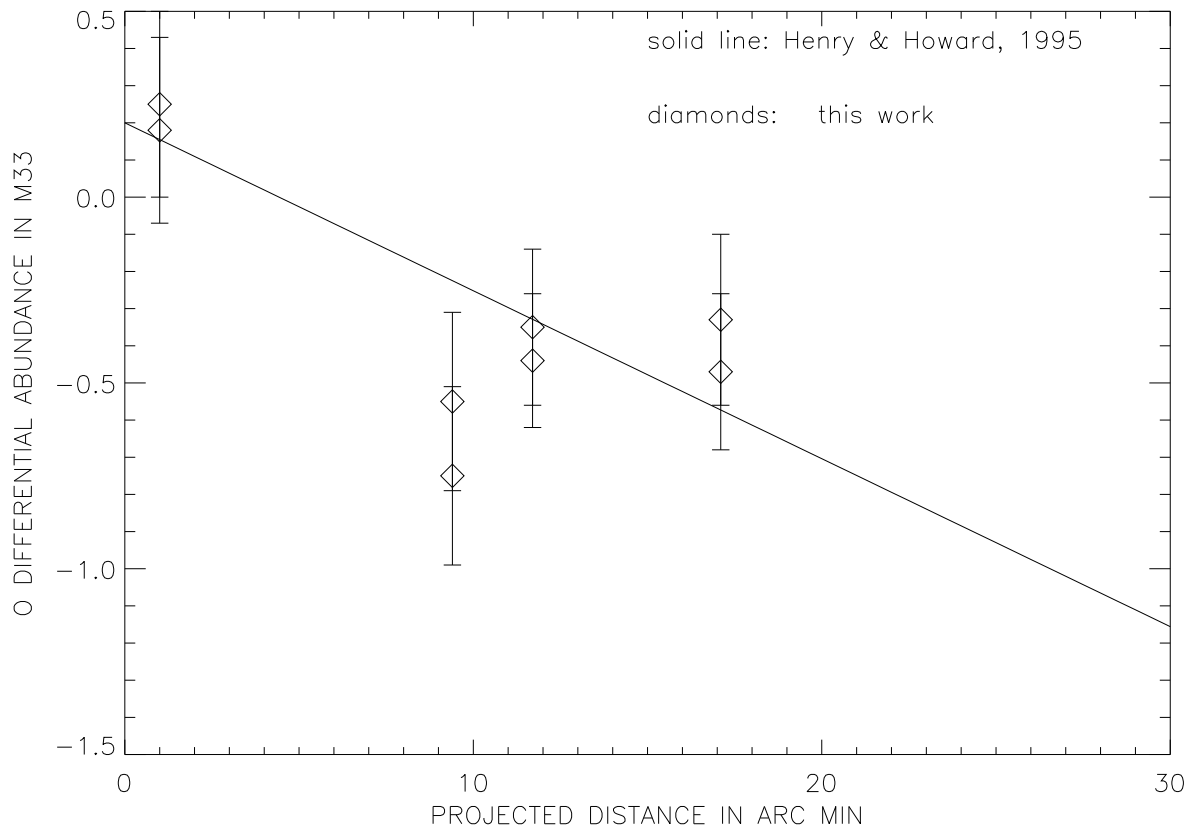


Fig. 14.— The O abundance gradient in M33 from stellar data. Symbols with the same abscissa values refer to the same object. The line represents the linear gradient derived by Henry & Howard (1995) from H II region data taken from different authors.

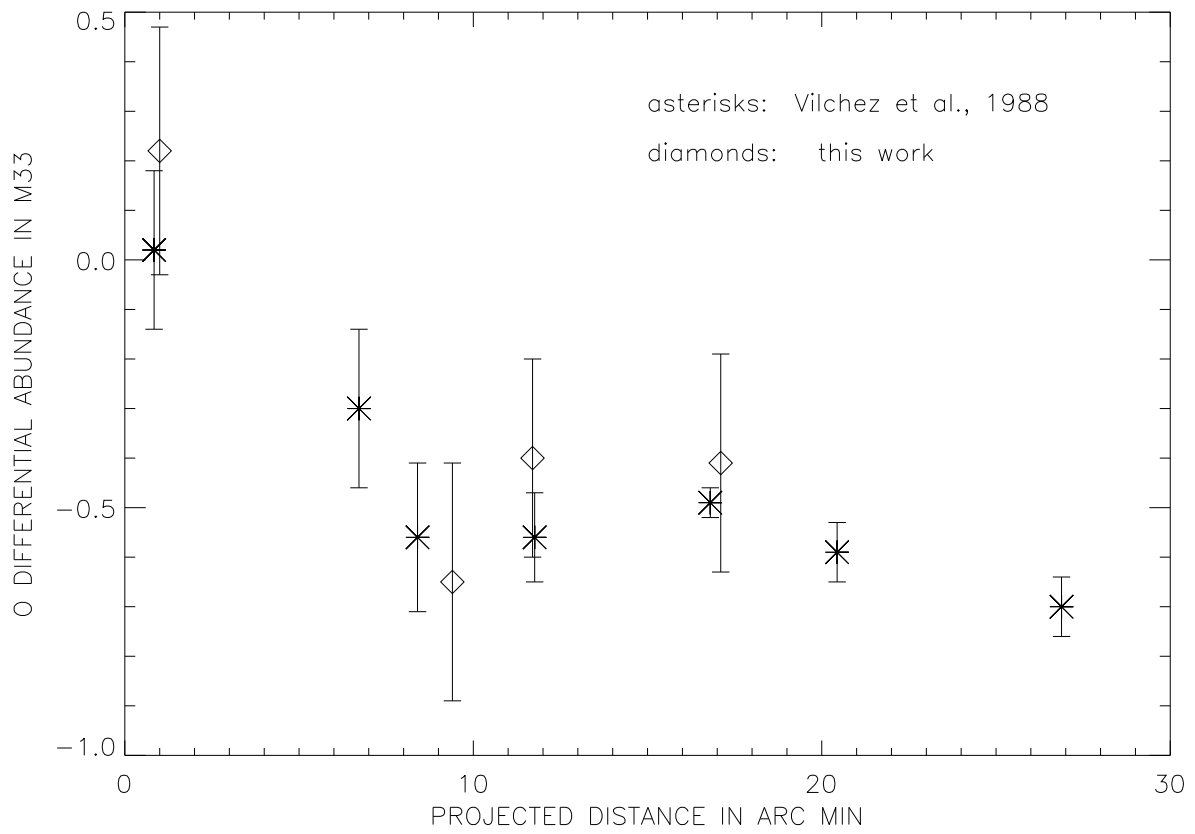


Fig. 15.— The differential abundance gradient in M33 for stars in this work (diamonds) and from H II regions (Vilchez et al. (1988)) We have used the average values given in Table 9 for clarity.

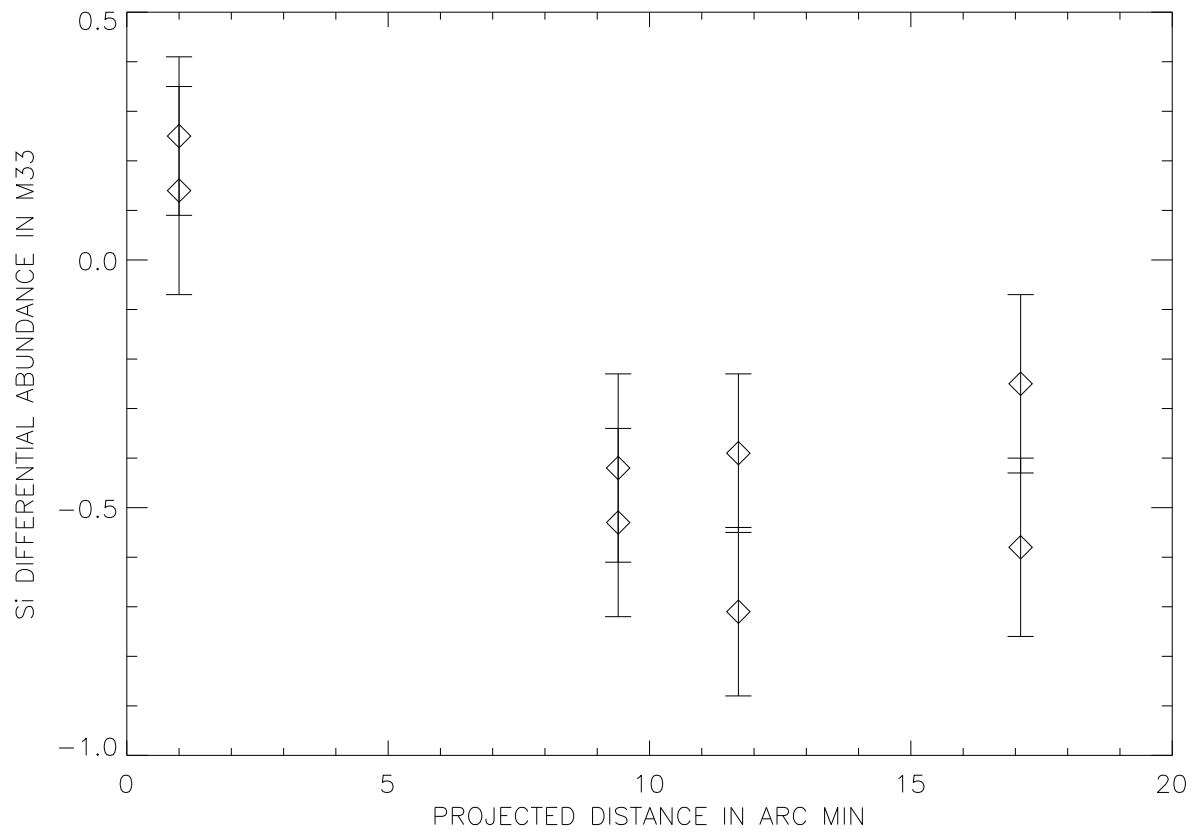


Fig. 16.— The Si abundance gradient in M33 from stellar data. Symbols with the same abscissa values refer to the same object.

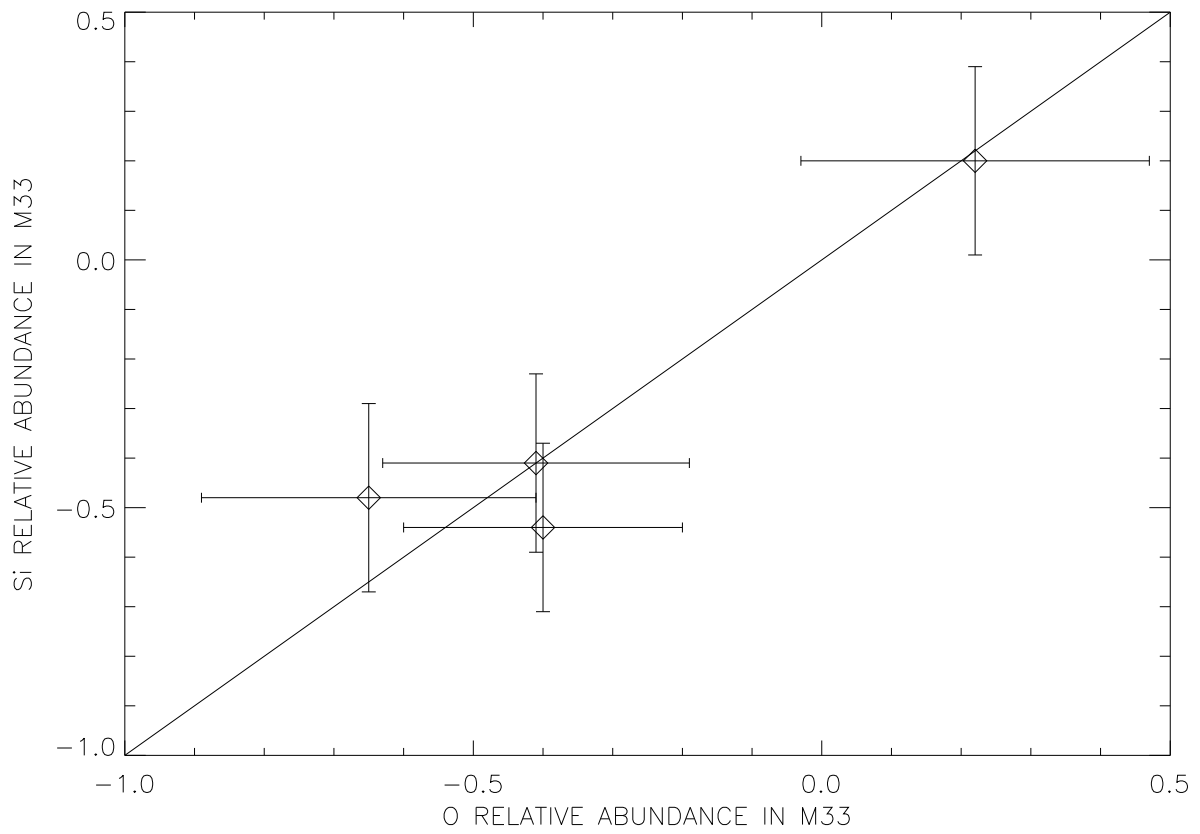


Fig. 17.— The correlation of the Si and O relative abundances in stars of M33 with respect to Galactic stars. The average values of for each individual object have been used for clarity.

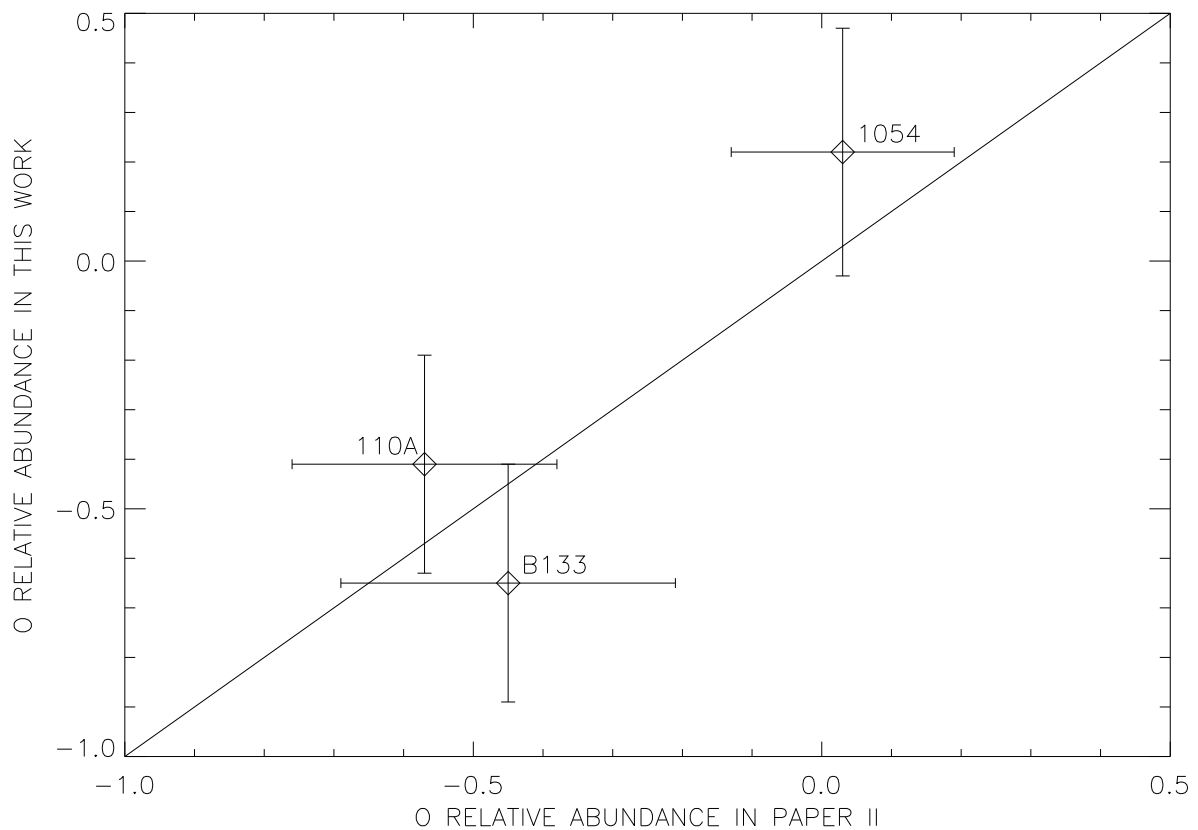


Fig. 18.— The relative O abundances obtained in Paper II and in this paper, for the three stars in common.